ENGINEERING RESEARCH INSTITUTE
THE UNIVERSITY OF MICHIGAN
ANN ARBOR

Scientific Report

SOME STUDIES OF THE DISCHARGE INITIATIONS IN A COLD-CATHODE GAS TETRODE

N. W. Spencer
R. C. Kiene
W. G. Dow

Project 2269

DEPARTMENT OF THE ARMY
DIAMOND ORDNANCE FUZE LABORATORIES
WASHINGTON, D. C.
CONTRACT NO. DAI-49-186-502-ORD-(P)-194

August 1957

TABLE OF CONTENTS

LIST OF FIGURES

LIST OF FIGURES
(Continued)

LIST OF FIGURES
(Concluded)

ABSTRACT

Studies related to the verification of a suggested equivalent circuit for the grid-cathode discharge in a subminiature cold-cathode gas tetrode have led to modification of the equivalent circuit, and to consideration of the firing time delays as basically a statistical matter. Further investigation is necessary before these conclusions can be firmly established.

OBJECTIVE

The purpose of this investigation was to obtain a better understanding of the fundamental reasons for delays occurring in the initiations of a low-level gas discharge.

1. INTRODUCTION AND ACKNOWLEDGMENTS

The Electrical Engineering Department of The University of Michigan has been conducting a study, primarily analytical, of certain properties of a subminiature, cold-cathode gas tetrode known as QF-391. Generally speaking, the investigations have been concerned with a particular circuit configuration using the tube which enables illustration of the readily observable property of a delay between application of a ramp function input current and breakdown of the control grid-cathode gap.

This research has been carried out for, and under sponsorship of, the Diamond Ordnance Fuze Laboratories. The QF-391 was developed by the Raytheon Electric Corporation under contract with the Diamond Ordnance Fuze Laboratories.

Several members of the staffs of the Electrical Engineering Department and the Diamond Ordnance Fuze Laboratories have contributed to this study. As is natural in a program to which different individuals contribute at different times, it is not always possible to give the proper credit for various aspects of the work. It is especially difficult in this case where some portions of the work have a bearing upon classified applications, and where some appropriate references are classified and thus cannot be noted.

The contributors from the Diamond Ordnance Fuze Laboratories include T. M. Liimatainen (scientific officer), Martin Reddon, Alfred Ward, and Jay Lathrop; from The University of Michigan, aside from those noted on the title page of this report, William Kerr, H. G. Hedges (now at Michigan State University), and Jules Needle (now at Northwestern University).

The bulk of the investigation discussed in this report was carried out by R. C. Kiene, now at Minneapolis-Honeywell, who was at the time a graduate student. Mr. Kiene likewise prepared much of the rough draft of this report.

2. THE EXPERIMENTAL CIRCUIT

In connection with certain classified work, it was observed that appreciable delays occur between the application of test signals to some cold-cathode gas-tetrode grid-cathode gaps and the breakdown of the gas in the gap. One of the circuits that illustrates the effect quite readily is shown in Fig. 2.1. In this example, a current source is employed to initiate the flow of

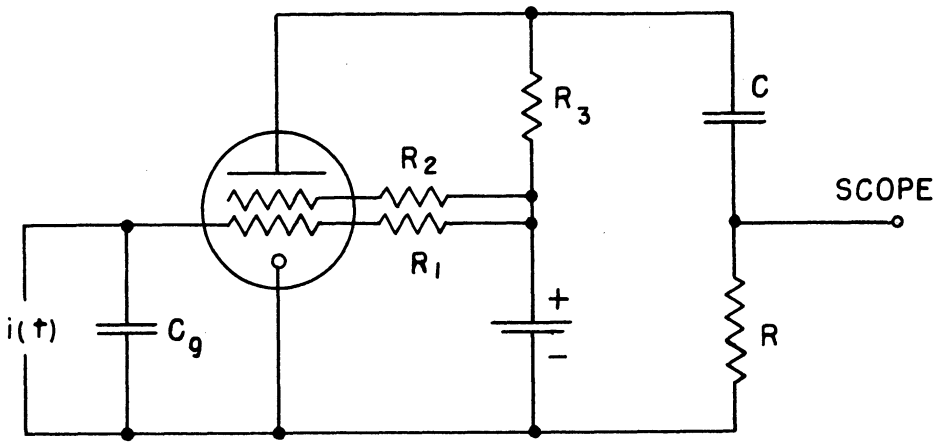

FIG. 2.1

EXPERIMENTAL CIRCUIT EMPLOYING

COLD-CATHODE GAS TETRODE

current in the g-c gap which operates, initially at least, in the Townsend region. The capacitance C_g is that associated with the current generator and test setup wiring. The plate and grid circuit elements and the battery are arranged to bias these tube elements appropriately, and to enable observation of breakdown by providing an easily observable magnitude of plate current. In operation, a current input signal is initiated which, after a delay, fires the g-c gap which in turn causes plate-cathode conduction and an indicating signal, for observation across R_5.

This circuit was chosen for study. The general objective was to (a) obtain an understanding of the factors governing the observed delays, and (b) establish the validity of an equivalent circuit that had been suggested to simulate the observed effects.

A current-type input signal is not always the most convenient experimentally; thus one of the first steps taken in this work was to arrange an equivalent voltage source. In this regard replace (Fig. 2.1) the current source i(t) and the shunt capacitance with a voltage generator e(t) and a series capacitance C_g by Norton's theorem. In substantiation, from Fig. 2.1 we can write:

$$i(t) = C_g \frac{de_1(t)}{dt} + i_1(t) \quad , \qquad (2.1)$$

$$e_1(t) = \frac{1}{C_g}\int i(t)dt - \frac{1}{C_g}\int i_1(t)dt \quad , \text{ and} \tag{2.2}$$

$$e(t) = e_1(t) + \frac{1}{C_g}\int i_1(t)dt \quad . \tag{2.3}$$

Equation 2.3 states that we can have equivalent voltage source e(t) operating in series with the capacitor C_g provided the voltage

$$e(t) = \frac{1}{C_g} i(t)dt \quad . \tag{2.4}$$

An assumption should be noted at this point. In changing from a current source to a voltage source equivalent circuit, the complete shunt capacitance C_g became a series capacitance. This step is something of an approximation. In an experimental setup of the test circuit, the capacitance C_g will consist of all capacitance to be found in parallel with the current generator including stray and tube capacitances. The stray and tube capacitances will of course always be present and can never be completely eliminated from the shunt branch and placed in a series circuit arrangement. These capacitances, although in a sense neglected here, have an effect, considered in Section 10, on the tube operation.

3. SIMPLIFICATION OF THE EXPERIMENTAL CIRCUIT

In this section, the equivalent circuit of the experimental circuit (Fig. 5.1) will be considered for possible simplifications. It can be demonstrated that the time interval between breakdown of the grid-cathode gap and anode-cathode gap is relatively small compared to the time interval between the application of the input signal and the grid-cathode breakdown. Accordingly, this study is confined to the time lag mechanism of the grid-cathode gap of the QF-391 gas tetrode. Thus the equivalent circuit may be reduced to that shown in Fig. 3.1, where the second grid and anode circuits of the tube are omitted. As a parallel, during bench testing, the anode and second grid-circuit parameters are maintained constant. Thus it is assumed that any contributions that these circuits might make to alter the time response of the grid-cathode circuit can be considered constant.

Typical static characteristics of the grid-cathode gap are shown in Fig. 3.3.* The operating point of the gap is usually chosen at some initial value of current such as i_o, if illustrating a typical breakdown point.

*Grid-to-Cathode Static Characteristics - Appendix IV.

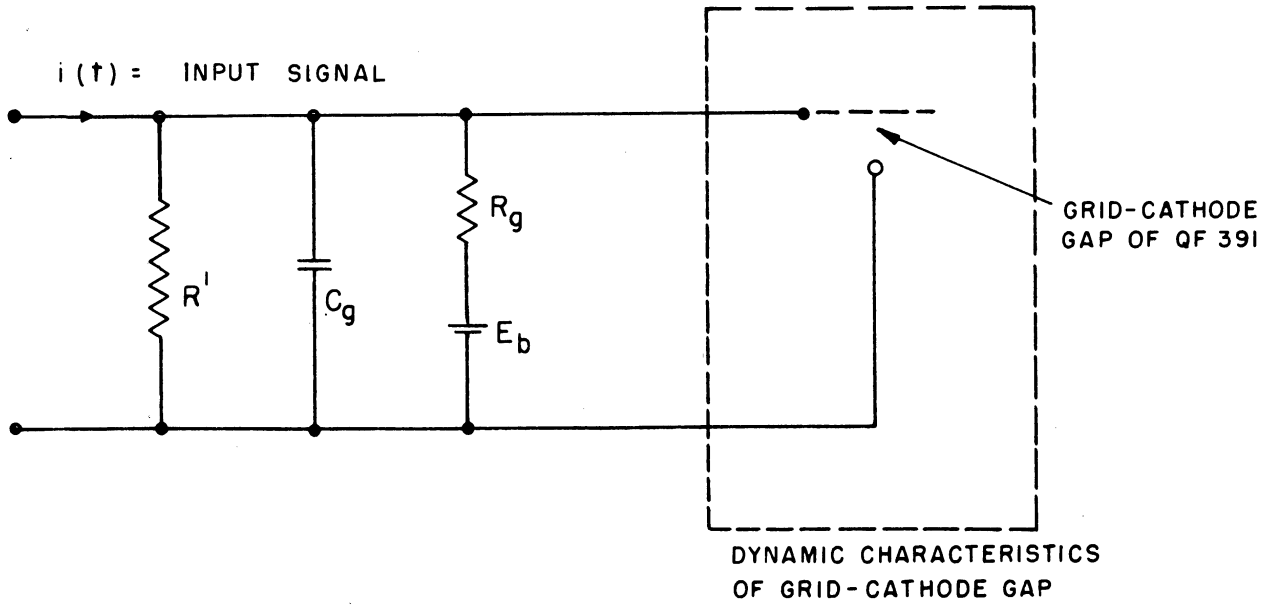

FIG. 3.1 EQUIVALENT CIRCUIT AFTER ELIMINATION OF ANODE AND SECOND GRID CIRCUITS

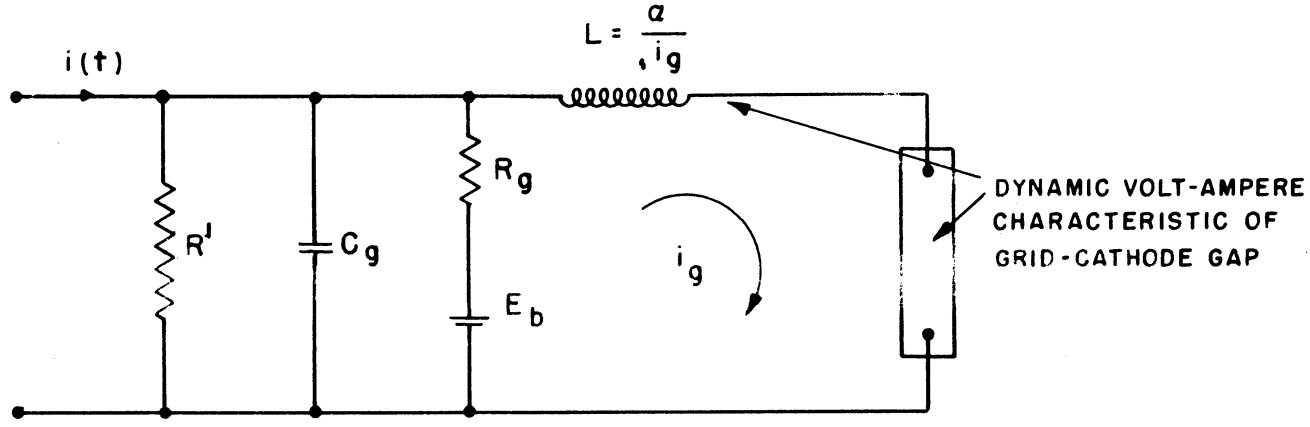

FIG. 3.2 EQUIVALENT CIRCUIT INCLUDING AN INDUCTANCE TO SIMULATE THE DYNAMIC TIME LAG CHARACTERISTIC OF THE GRID-CATHODE GAP

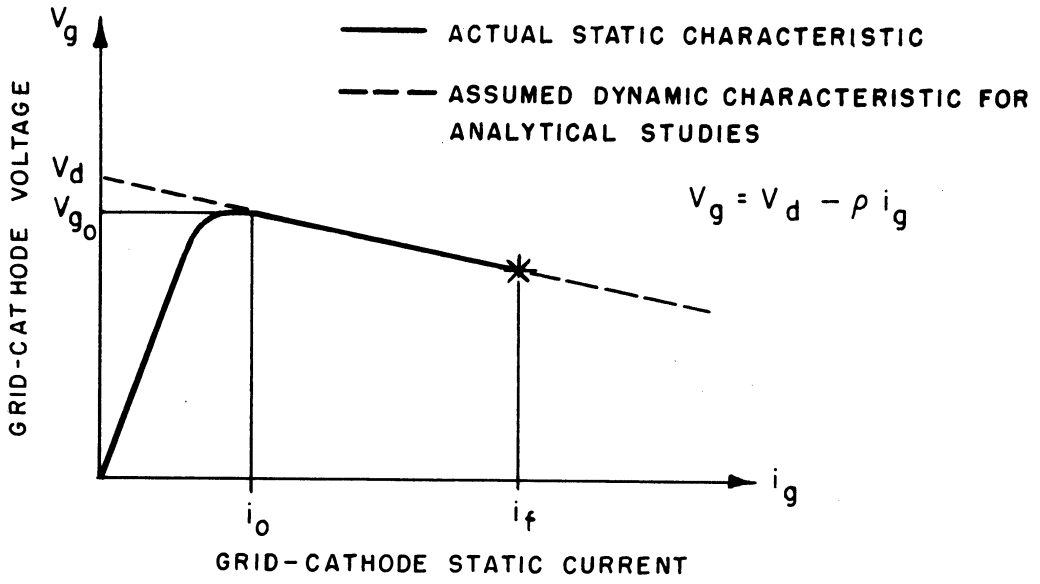

FIG. 3.3 TYPICAL GRID-CATHODE STATIC CHARACTERISTICS

When the imput signal is applied to the grid circuit, the increasing current through the grid-cathode gap does not follow the static characteristics shown, but instead a dynamic characteristic (Fig. 3.2) which depends on the tube constants and the ionization mechanism of the gap. The current buildup across a gaseous gap operating in the Townsend region of the static characteristics can presumably be explained by a dynamic volt-ampere characteristic and in part simulated by an inductance whose magnitude varies inversely with the current. The parameter is defined as

$$L = \frac{\alpha}{i_g} \tag{3.1}$$

where α is a constant dependent upon gas parameters.

The dynamic resistance of the grid-cathode gap is a function of the current through the gap. However, as a first approximation, this resistance is considered to have a constant magnitude ρ corresponding to the negative slope of the static characteristic, since operation of the tube is confined largely to this region in all experimental investigations. Then, assuming ρ as the constant dynamic resistance of the gap, we obtain a relationship from the linear portion of the volt-ampere curve of Fig. 3.3, that is, for $i > i_o$,

$$V_g = V_d - \rho i_g \ . \tag{3.2}$$

Thus considering both the negative resistance and special inductance, the grid circuit of the test circuit has the form shown in Fig. 3.4, retaining, for the moment, the current generator form. (Figure 3.5 illustrates the voltage source equivalent circuit.)

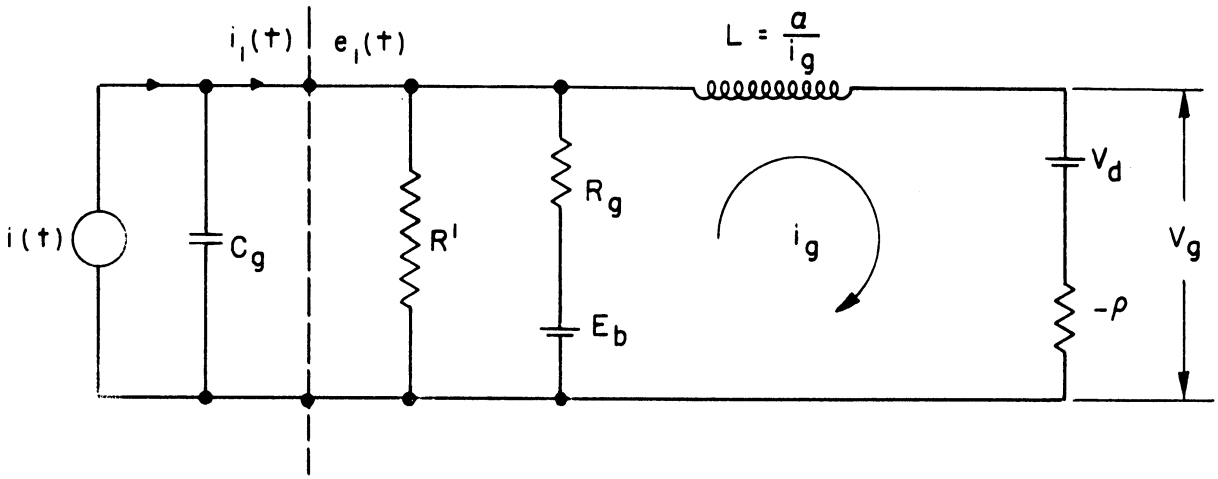

FIG. 3.4 EQUIVALENT CIRCUIT WITH ASSUMED DYNAMIC-VOLT-AMPERE CHARACTERISTIC FOR GRID-CATHODE GAP

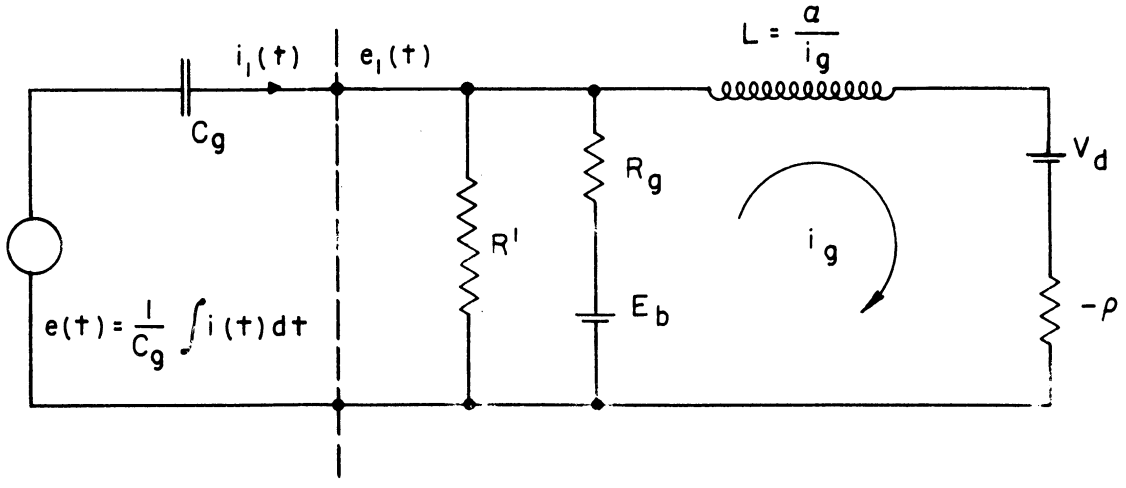

FIG. 3.5 VOLTAGE SOURCE EQUIVALENT CIRCUIT OF FIG. 3.4

The resistance of the parallel combination of R', circuit leakage resistance, and R_g, grid circuit resistance, as compared with the rest of the circuit, is very high; thus these branches can be neglected. The battery V_d can also be ignored, since its effect is only that of setting the initial condition i_o in the tube. The elimination of these parameters has no appreciable effect on the dynamic response of the equivalent circuit; however, it must be remembered that the inductance L has an initial value corresponding to the initial condition $i = i_o$.

The resulting simplified equivalent circuit employed to simulate the dynamic properties of the test circuit is shown in Fig. 3.6. Through analysis of this circuit, the time interval required for the current to increase from i_o to i_f will be determined. For this purpose a relationship between this time interval as a function of e(t) and the differential equation describing the current i_g in this circuit will be developed.

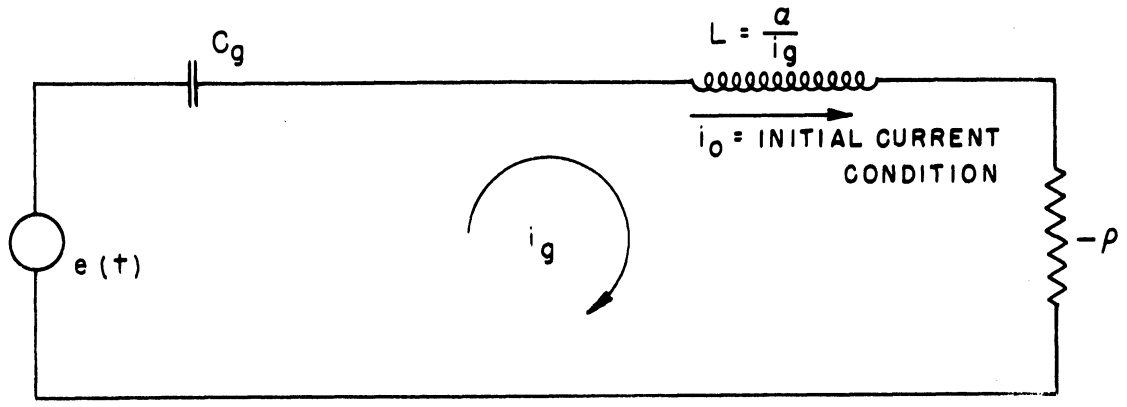

FIG. 3.6 FINAL EQUIVALENT CIRCUIT SIMULATING THE DYNAMIC CHARACTERISTICS OF THE GRID-CATHODE CIRCUIT OF THE TYPE QF-391 TUBE

4. NONLINEAR DIFFERENTIAL EQUATION DESCRIBING CURRENT IN EQUIVALENT CIRCUIT

Having determined the simplified equivalent circuit for simulating the dynamic characteristics of the fuze circuit, we proceed to solve for the current i_g as a function of the various parameters. Due to the variable inductance in the equivalent circuit, the differential equation describing the current is nonlinear:

$$\left(\frac{\alpha}{i_g}\right) \frac{di_g}{dt} - \rho\, i_g + \frac{1}{C_g} \int i_g\, dt = e(t) \quad . \tag{4.1}$$

The initial condition of this equation at time t = 0 is that

$$i_g = i_o \quad . \tag{4.2}$$

Differentiating Eq. 4.1 to remove the integral, we obtain a second-order nonlinear differential equation:

$$\left(\frac{\alpha}{i_g}\right)\frac{d^2 i_g}{dt^2} - \left(\frac{\alpha}{dt^2}\right)\left(\frac{di_g}{dt}\right)^2 - \rho\frac{di_g}{dt} + \frac{1}{C_g} i_g = \frac{d\,e(t)}{dt} \tag{4.3}$$

$$\left(\frac{\alpha}{i_g}\right)\frac{d^2 i_g}{dt^2} - \left[\left(\frac{\alpha}{i_g^2}\right)\frac{di_g}{dt} + \rho\right]\frac{di_g}{dt} + \frac{1}{C_g} i_g = \frac{d\,e(t)}{dt} \quad . \tag{4.4}$$

Modest attempts to solve this equation analytically were not fruitful; however, through use of a graphical approach, the phase-plane method, a solution was determinable. It is feasible to obtain a solution through use of an analog computer; thus, during the course of the investigation described in this report, a solution was obtained in that manner also. The analog computer setup of Eq. 4.1 is given in Section 7.

5. BREAKDOWN DATA FOR TEST CIRCUIT FOR $e(t) = \lambda t$

The dynamic behavior of the test circuit was investigated experimentally by applying a particular voltage signal and firing the tube. The voltage signal employed* had the form

$$e(t) = \lambda t \quad , \tag{5.1}$$

and was used because of its relative simplicity.

The experimental test-circuit arrangement used to obtain the dynamic firing characteristics as a function of λ is shown in Fig. 5.1. The battery λ and the resistance R_1—capacitance C_1 combination generated the voltage $e(t) = \lambda t$. Since the tube fired after relatively short time intervals (in the 0-50-millisecond range), a simple R_1C_1 combination could be used to generate the λt signal. The voltage appearing across the capacitance (C_1) has a linear slope of λ_1/R_1C_1 at t = 0. Also, for small time intervals below the R_1C_1 time constant, the slope is nearly the same. Therefore, by making the time constant R_1C_1 equal to, say, 1 second, the voltage rise across the condenser can be considered just λt for short time intervals.

*Use suggested by DOFL personnel.

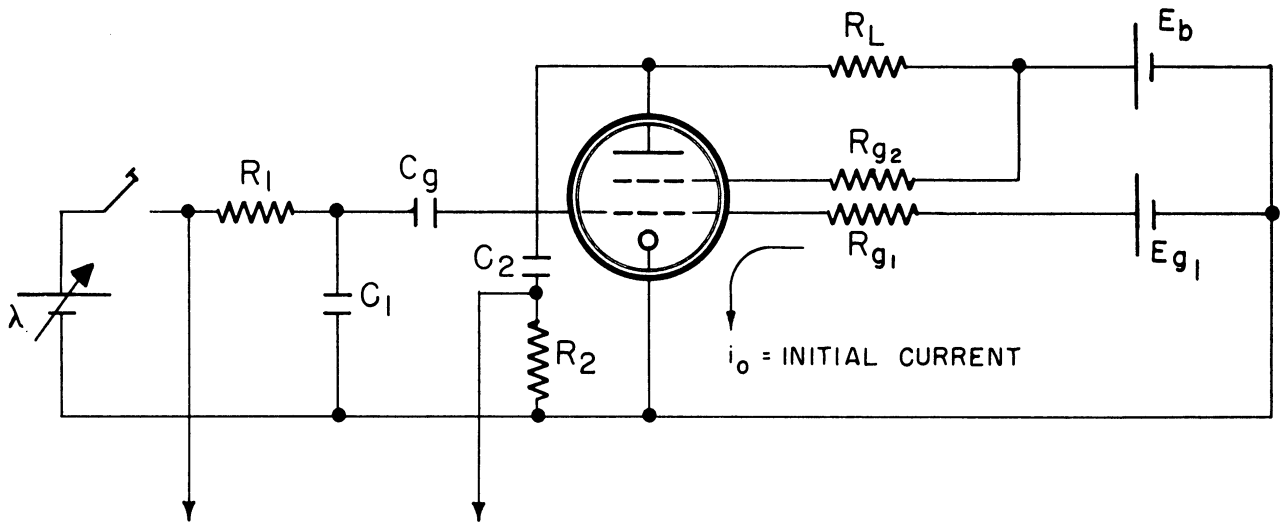

CIRCUIT VALUES:

TUBE - QF-391 NO. 4092 LOT 8N1

λ - VARIABLE VOLTAGE FOR ADJUSTING VALUE OF LINEAR RATE OF RISE VOLTAGE APPLIED TO TUBE.

$R_1 = 1 \times 10^6$ OHM	$E_b = 180$ VOLTS
$C_1 = 1 \times 10^{-6}$ FARAD	$E_{g1} = 155$ VOLTS
$C_g = 10 \times 10^{-12}$ FARAD	$R_{g2} = 1 \times 10^{10}$ OHM
$C_2 = .05 \times 10^{-6}$ FARAD	$R_{g1} = 1 \times 10^{10}$ OHM
$R_2 = 50 \times 10^3$ OHM	$i_o = 5.4 \times 10^{-9}$ OHM (INITIAL CURRENT)
$R_L = 6.8 \times 10^6$ OHM	

FIG. 5.1 EXPERIMENTAL SETUP FOR OBTAINING DYNAMIC CHARACTERISTIC OF TEST CIRCUIT

The capacitance C_g represents the total input capacitance as shown in Fig. 3.6, and has a value of 10 μμ farads. The various values of the other parameters are given in Fig. 5.1.

Operation of the circuit is as follows. E_{g1} is adjusted until an initial current i_o (steady) flows through the grid-cathode gap of the QF-391. When the switch is thrown, voltage λ is applied to the R_1C_1 combination and, for the small time interval of interest, the voltage across C_1 is λt, a linear rate of rise signal. At the same time the switch is thrown, a signal is applied to an oscilloscope to initiate the time-calibrated horizontal sweep. When the tube fires, evidence of the fact appears on the face of the scope as a vertical displacement. From the horizontal distance traveled by the beam up to the time of firing, the time delay between the applied signal and firing can

be determined. Typical results are plotted in Fig. 5.2 where computed curves (to be described) are included for comparison.

The points plotted represent the results of experimental data for one tube at a particular value of operating or initial current i_o. It was noticed in obtaining these data that the firing time was not a unique function of a particular value of λ, as might be expected, but rather a statistical function. Thus the points plotted on Fig. 5.2 represent an average firing time for twenty firings at each different value of λ. The statistical nature of firings makes it difficult to obtain a unique curve to represent the dynamic characteristic of the fuze circuit.

The curve shown is a function of the tube's characteristics and of the chosen boundary conditions. By trying many tubes, most of the results indicate the general shape of the curve shown for initial values of operating current near $i_o = 10^{-9}$ amp and firing currents of $i_f = 10^{-8}$ amp and greater. The only region which shows appreciable divergence is for low values of λ near the "forbidden region," defined as a range of values of λ below which the tube ceases to fire.

For the particular tube shown, the lowest value of λ at which the tube fired was $\lambda_f = 1.5 \times 10^2$ volts/sec. The time delay between application of this λ_f and firing was T = 70 milliseconds. In general, for the operating regions of interest between 10^{-9} amp to 10^{-8} amp the forbidden region varies from $\lambda = 1.0 \times 10^2$ volts/sec to $\lambda = 10^3$ volts/sec with the forbidden region firing times ranging from 80 milliseconds to about 10 milliseconds, respectively.

The curve shown in Fig. 5.2 should not be considered a unique representation of the dynamic characteristics of the circuit, but instead an average picture showing the general character of operation. For the initial stages of our investigations with the equivalent circuit, this experimental curve was used as a basis of comparison for the equivalent circuit results. This enabled us to obtain a rough value for the nonlinear inductance to be used in the equivalent circuit. The dashed curve of Fig. 5.2 represents the type of dynamic data which it was desired to simulate by the equivalent circuit of Fig. 3.6.

6. CORRELATION OF EXPERIMENTAL AND LINEARIZED EQUIVALENT CIRCUIT DATA

After the experimental data shown on Fig. 5.2 were obtained, the equivalent circuit response was investigated in hope that a correlation between the experimental and analytical data could be found. However, prior to this, a similar linear circuit with a constant inductance was solved in anticipation of "bounding" the experimental results. This "bounding" property of the linear circuit can be explained as follows.

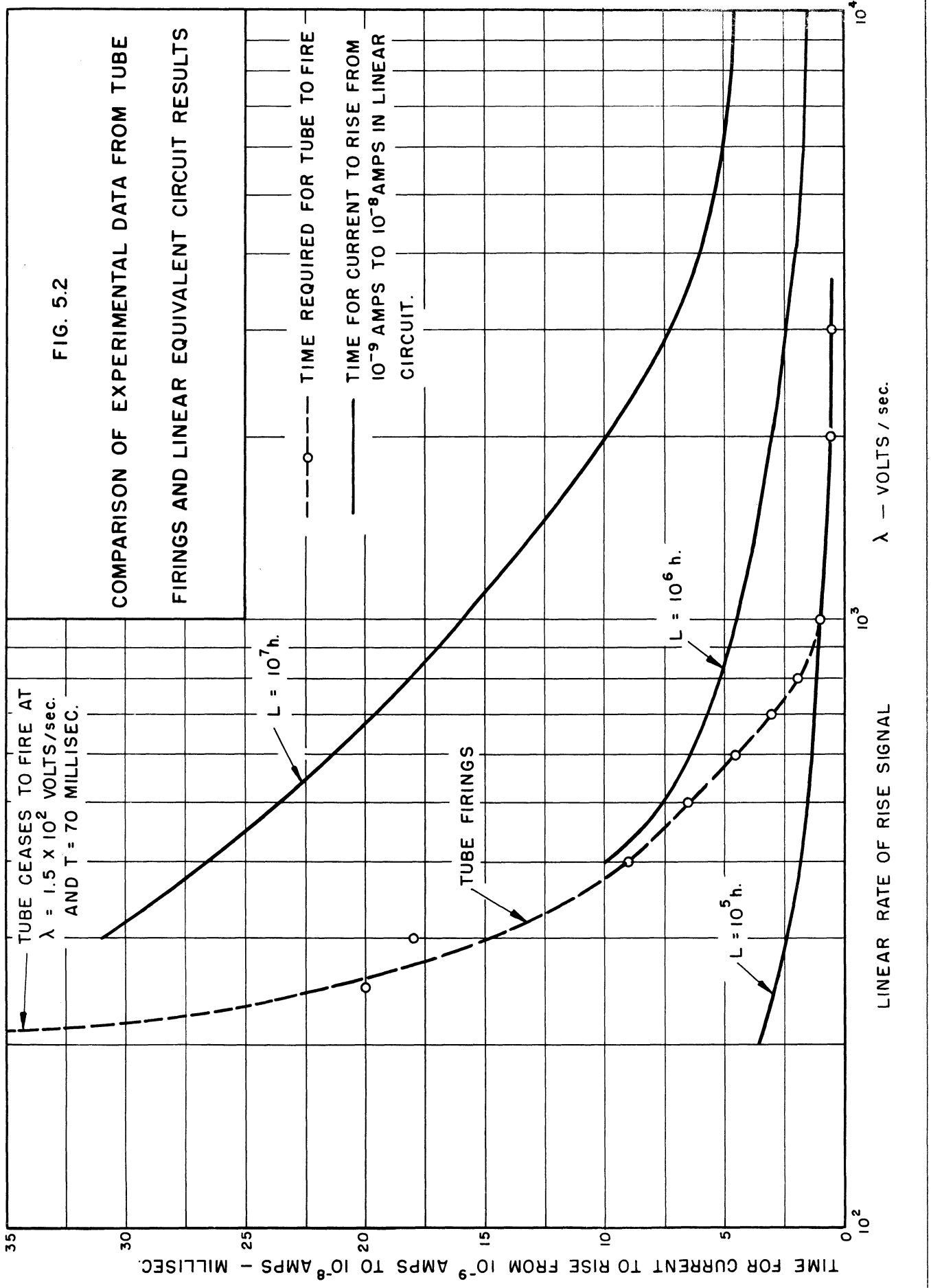
FIG. 5.2
COMPARISON OF EXPERIMENTAL DATA FROM TUBE FIRINGS AND LINEAR EQUIVALENT CIRCUIT RESULTS
TIME REQUIRED FOR TUBE TO FIRE
TIME FOR CURRENT TO RISE FROM 10^{-9} AMPS TO 10^{-8} AMPS IN LINEAR CIRCUIT.
TUBE CEASES TO FIRE AT $\lambda = 1.5 \times 10^2$ VOLTS/sec. AND T = 70 MILLISEC.
L = 10^7 h.
L = 10^6 h.
L = 10^5 h.
TUBE FIRINGS
TIME FOR CURRENT TO RISE FROM 10^{-9} AMPS TO 10^{-8} AMPS - MILLISEC.
LINEAR RATE OF RISE SIGNAL
λ — VOLTS / sec.
35
30
25
20
15
10
5
0
10^2
10^3
10^4

In the nonlinear equivalent circuit, the range of values over which the nonlinear inductance varied (determined by the current) was unknown. A rough value for this inductance can be computed readily, but for the particular tube used, this value was inadequate. In testing various tubes it was found that the range of current variation across the grid-cathode gap was from about $i_o = 10^{-9}$ amp to the breakdown current of approximately $i_f = 10^{-8}$ amp. Therefore, the proposed nonlinear inductance function $L = \alpha/i_g$ used in the equivalent circuit would vary by a factor of 10 in this current range. This assumes that the current i_g increases continuously from i_o to i_f and no discontinuities of the function $L = \alpha/i_g$ are encountered. Thus the dynamic characteristics of the nonlinear circuit could presumably be considered "bounded" by the characteristics of two linear circuits using the maximum and minimum values of the nonlinear element $L = \alpha/i_g$ instead of the varying inductance. By this method the experimental curve shown in Fig. 5.2 can be treated as "bounded" by the linear equivalent circuit's results as shown. In this way, the range of values in which the nonlinear element $L = \alpha/i_g$ had to vary was established.

The linear circuit which was used is shown in Fig. 6.1 accompanied by the analog computer setup (Fig. 6.2) used to simulate the circuit. As noted, the inductance did not vary with current i_g as in the nonlinear case, but was maintained constant.

The equation of the circuit is

$$L \frac{di_g}{dt} - \rho\, i_g + \frac{1}{C_g} \int i_g\, dt = \lambda t \quad , \tag{6.1}$$

where

$$i_g = i_o \text{ at time } (t) = 0 \quad . \tag{6.2}$$

The solution of this linear differential equation is

$$i_g = \frac{\lambda}{L} \left[\frac{1}{\beta_o^2} + \frac{1}{\beta_o \beta} e^{+\alpha t} \sin (\beta t - \psi) \right] + i_o \left[\frac{\beta_o}{\beta} e^{+\alpha t} \sin (\beta t + \psi) \right] , \tag{6.3}$$

where

$$\alpha = \frac{\rho}{2L} \quad ,$$

$$\beta = \sqrt{\frac{1}{LC} - \frac{\rho^2}{4L^2}} \quad ,$$

$$\psi = \tan^{-1} \frac{\beta}{\alpha} \quad , \text{ and}$$

$$\beta_o^2 = \alpha^2 + \beta^2 \quad .$$

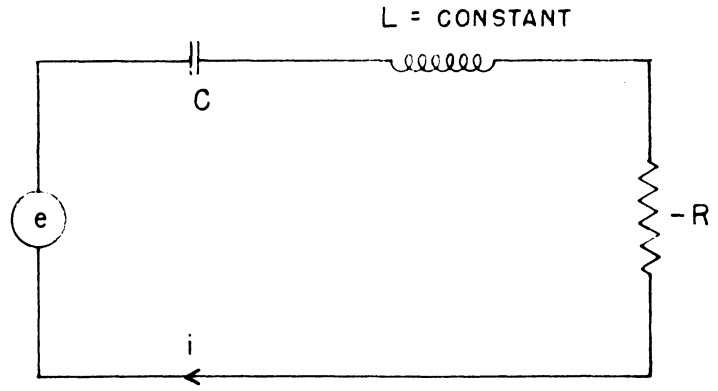

FIG. 6.1 CIRCUIT INVOLVING LINEAR INDUCTANCE AND NEGATIVE RESISTANCE

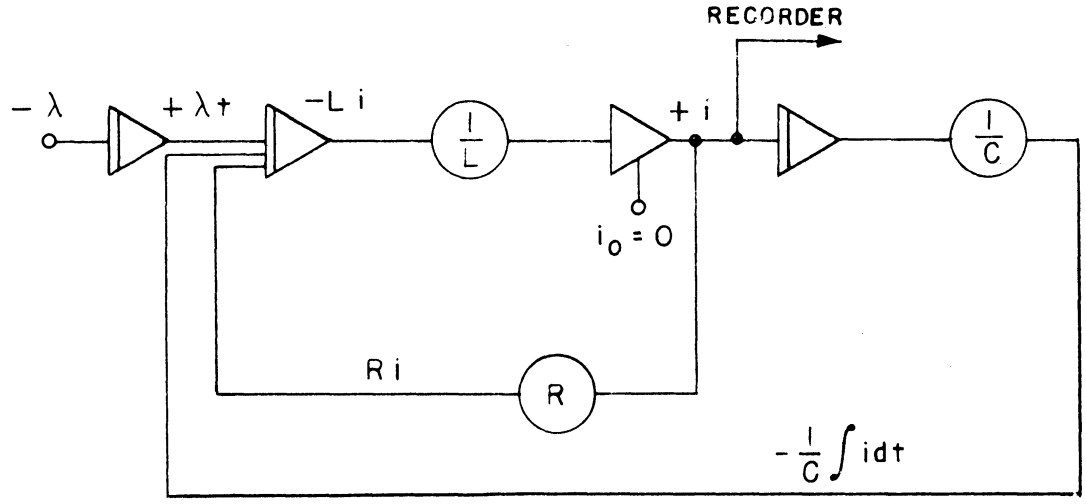

FIG. 6.2 NORMALIZED COMPUTER SETUP FOR SOLUTION OF CURRENT IN EQUATION 4.1

The curves shown in Fig. 5.2 are for the following values of the linear circuit's parameters.

$$\lambda = 10^2 \text{ to } 10^4 \text{ volts/sec}$$

$$L = 10^5, 10^6, \text{ and } 10^7 \text{ henries}$$

$$C_g = 10 \times 10^{-12} \text{ farads}$$

$$\rho = -10^8 \text{ ohms} .$$

The solid curves of Fig. 5.2 represent the time it takes the current i_g to increase from an initial value of $i_o = 10^{-9}$ amp to a firing current $i_f = 10^{-8}$ amp for various values of λ. The results obtained from the linear circuit indicate that the experimental data are bounded for $L = 10^7$ to 10^5 henries. For values of λ greater than 10^3 volts/sec, the experimental results correspond very closely to $L = 10^5$ henries. For lower values of L, close to the forbidden region, there is a greater variation between the experimental and analytical data.

To discuss the correlation between the experimental curve shown in Fig. 5.2 and the curves describing the linear equivalent circuit, three curves are drawn in Fig. 6.3 to show the effect of varying L and λ. As can be inferred from Eq. 6.3, the current i_g is oscillatory and exponentially increasing in nature. With λ sufficiently high, the current in the equivalent circuit rises to a much greater value than $i_f = 10^{-8}$ amp during the first peak or oscillation. This can be considered as corresponding to the grid-cathode current reaching the breakdown current i_g before the first peak or oscillation occurs. With λ at some lower value such as λ_2, the current just reaches 10^{-8} amp during the first peak. This corresponds to the boundary of the forbidden region, that is, the lowest value of λ needed for the tube to fire on the first oscillation. When λ is reduced to less than λ_2, the current no longer reaches 10^{-8} amp during the first peak, but can exceed 10^{-8} amp during some later cycle. Thus, when $\lambda = \lambda_3$, λ can be associated with values which lie in the forbidden region, λ_2 representing the edge of the forbidden region. Also to be noted from the equations and curves is the fact that the time to reach 10^{-8} amp decreases with increasing λ, which is likewise observed experimentally.

The curves shown in Fig. 6.4 are for constant λ and variable inductance L. As the value of L is increased, the resonant frequency of the circuit decreases, consequently resulting in a greater time required for the current to reach $i_f = 10^{-8}$. Similarly, as can be seen from the curves of Fig. 5.2, when L is increased, the time required for the current to reach 10^{-8} amp, for the same constant value of λ, also increases.

From the bounding of the experimental data by the linear equivalent circuit data, it can be seen that the nonlinear function $L = \alpha/i_g$ should probably vary from 10^5 to 10^4 henries for high values of λ. For lower values of λ,

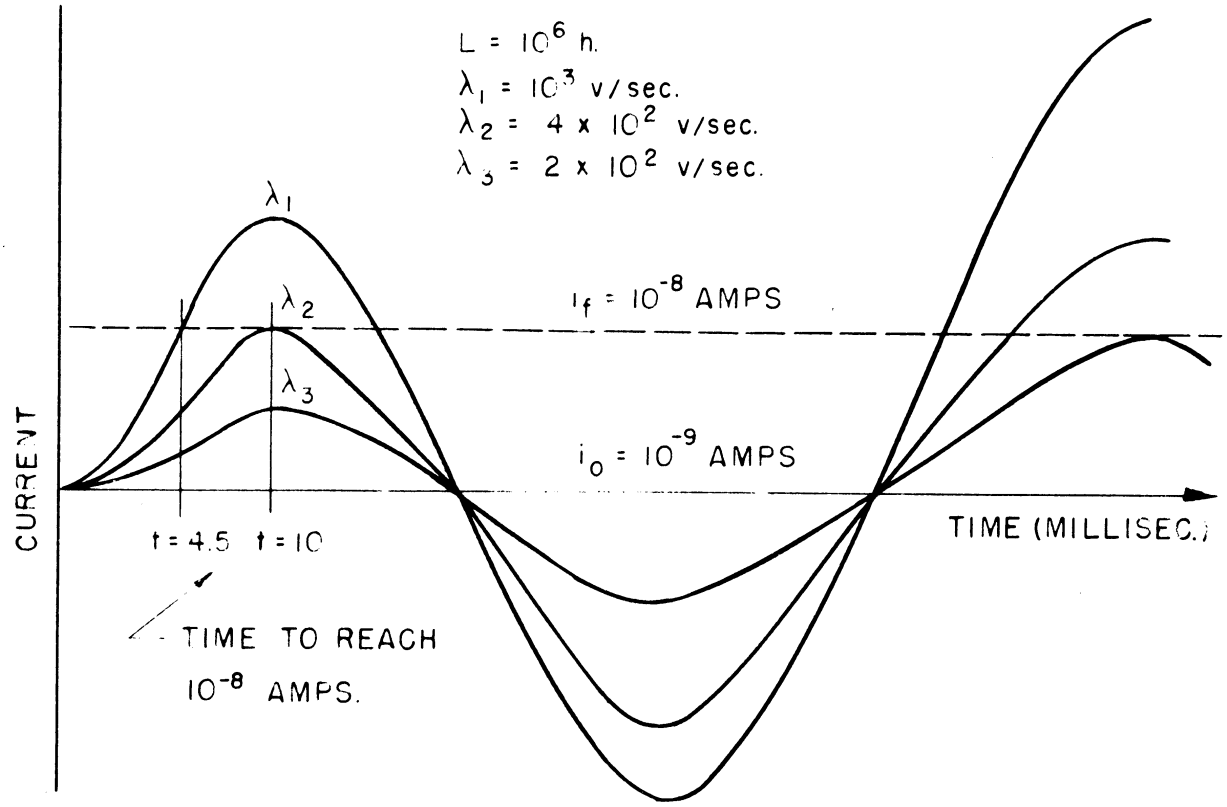

FIG. 6.3 CURVES SHOWING EFFECTS OF DIFFERENT VALUES OF λ ON CURRENT VARIATION IN LINEAR CIRCUIT.

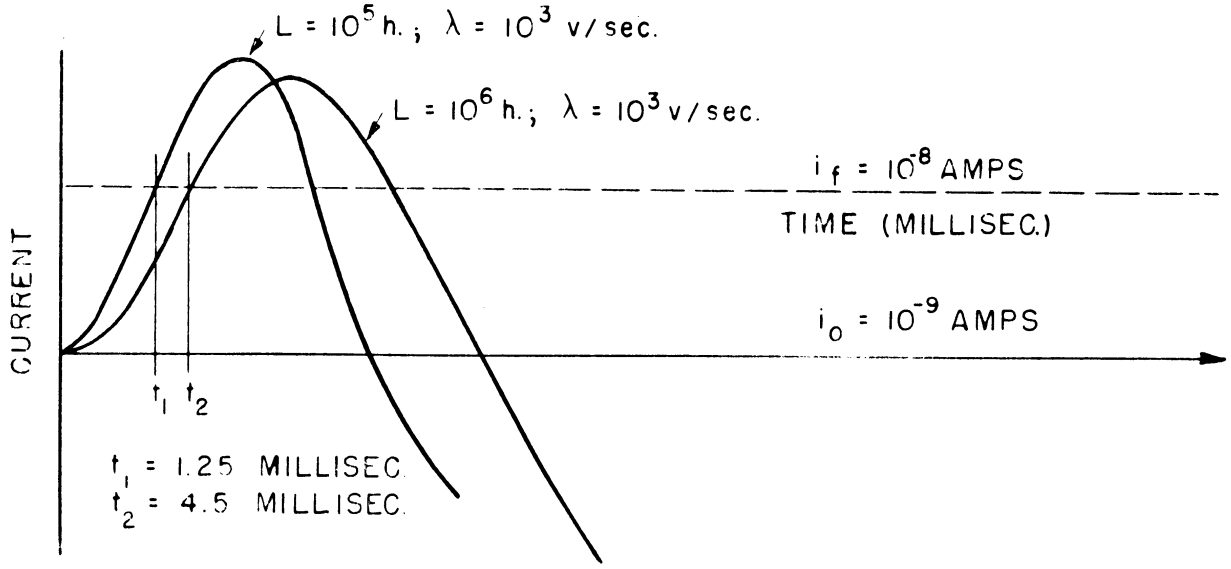

FIG. 6.4 CURVES SHOWING EFFECTS OF DIFFERENT VALUES OF (L) WITH CONSTANT (λ)

some other range of greater L seems to be necessary. To investigate this point further, we now examine the nonlinear circuit of Fig. 3.6.

7. CORRELATION OF EXPERIMENTAL AND NONLINEAR EQUIVALENT CIRCUIT DATA

In the previous section it was shown that the experimental data of the test circuit could be "bounded" by analytical results obtained from the linear circuit of the form in Fig. 6.1. From these results, the range of values over which the nonlinear parameter $L = f(i_g)$ would have to vary to approximate the experimental data is determined. However, the exact variation of this function is unknown.

In this section the initially proposed nonlinear function $L = \alpha/i_g$ is studied with regard to its effect on the dynamic characteristics of the circuit shown in Fig. 7.1. The dynamic characteristics of the nonlinear circuit are then compared with the experimental and linear circuit data. The effects of several other types of nonlinear variations of the inductance parameter are also considered, and the results of employing these nonlinear inductances are compared with the experimental results for possible better correlation.

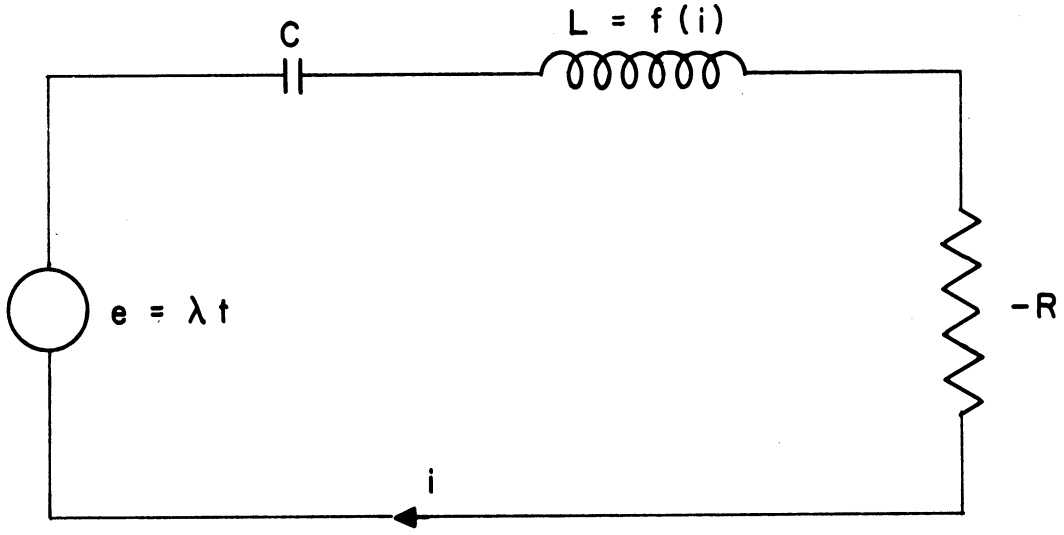

FIG. 7.1 SIMPLIFIED CIRCUIT INVOLVING NON-LINEAR INDUCTANCE AND NEGATIVE RESISTANCE

To solve the nonlinear equation describing the current variation in the equivalent circuit, an analog computer is used. Since the equivalent circuit is considered with various nonlinear inductances, Eq. 4.1 is put in the following general form:

$$f(i_g)\frac{di_g}{dt} - \rho\, i_g + \frac{1}{C_g}\int i_g\, dt = \lambda t \quad . \tag{7.1}$$

The corresponding computer equation is:

$$\frac{di_g}{dt} = \frac{1}{f(i_g)}\left(\rho\, i_g - \frac{1}{C_g}\int i_g\, dt + \lambda t\right) \quad . \tag{7.2}$$

After normalizing this equation, the computer setup for the solution of i_g as a function of time was arranged as shown in Fig. 7.2. Appendix III briefly explains the operation of this setup.

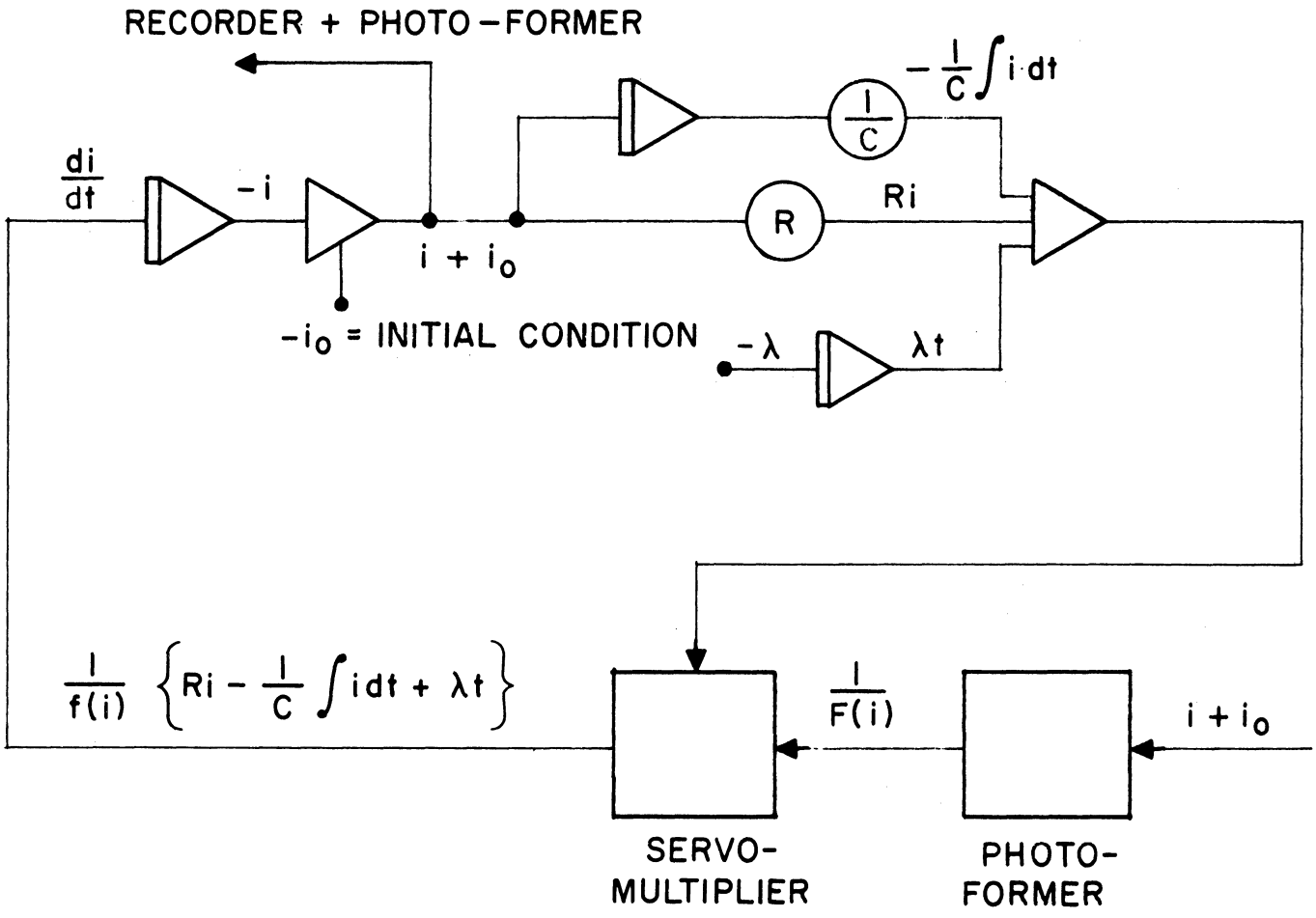

FIG. 7.2 NORMALIZED COMPUTER SETUP FOR SOLUTION OF CURRENT IN EQUATION 7.2.

7.1 VARIATION OF THE NONLINEAR INDUCTANCE AS $L = \alpha/i_g$

In Section 3 it was shown that the nonlinear element simulating the time lag of current buildup across the grid-cathode gap could have the form $L = \alpha/i_g$.

Having determined a range of variation of L (Section 6), an approximate value for the constant α can be calculated. Thus from the results obtained using a constant L, it is seen that, to approximate the test circuit's characteristics for low values of λ, the nonlinear element would have to vary from about 10^5 to 10^6 henries. This means that since the corresponding current range is from $i_o = 10^{-9}$ amp to $i_f = 10^{-8}$ amp, the coefficient of the di_g/dt term would vary as

$$f(i_g) = \frac{\alpha}{10^{-9}} \text{ to } \frac{\alpha}{10^{-8}} = \frac{10^{-3}}{10^{-9}} \text{ to } \frac{10^{-3}}{10^{-8}} = 10^6 \text{ to } 10^5 \text{ henries} .$$

The characteristics of the nonlinear circuit for two values of α are shown in Fig. 7.4 in comparison with experimental and linear circuit data to illustrate the boundary effect of the assumed linear circuit arrangement. Figure 7.3 shows the current variation of the linear circuit and the nonlinear circuit where $L = \alpha/i_g$. The curves are drawn for values of λ for which the current i_g just reaches the firing current i_f during the first peak. For lower values of λ, the current variation i_g will not reach the value i_f on the first peak but on some later peak, and, as previously defined, these values of λ lie in the forbidden region. It is of interest to note that the current i_g varies monotonically from i_o to i_f without discontinuity, and of particular interest that this representation shows clearly how the element of chance is a factor in the operation of this tube.

By observing the current variation of the nonlinear circuit in comparison with the linear case, it can be seen that the bounding effect concept of the linear case is not valid for times greater than that to the first peak, for the reason that the inductance seems to become infinite as the current passes through zero. This aspect of the problem has not been pursued other than to note the above. Actually it may prove upon investigation that the apparent passing through zero of the current is erroneous, resulting from assumptions in establishing the computer setup, and that in fact the current only approaches zero, as suggested by the flattening of the dashed curve of Fig. 7.3.

The presence of the second appearing peak is real and is observed in the experimental setup, as will be considered later.

The time required for the current i_g to reach i_f for the nonlinear and linear cases as a function of λ is shown in Fig. 7.4. As an illustration of the relationship between Figs. 7.3 and 7.4, the boundary value of λ is $\lambda = 5.0 \times 10^2$ volts/sec and $\lambda = 4.0 \times 10^2$ volts/sec for the nonlinear $L = 0.01/i_g$

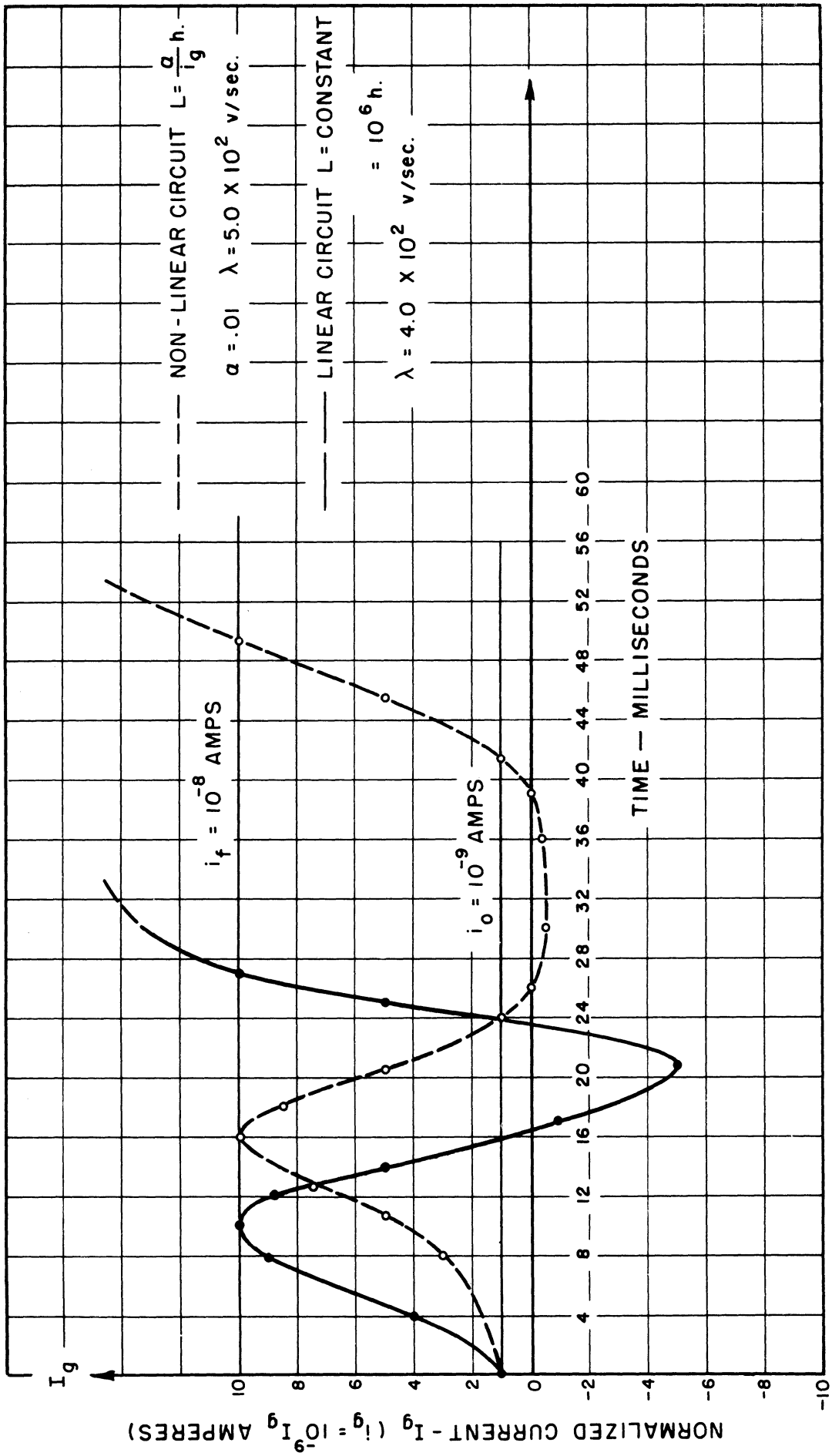

FIG. 7.3 COMPARISON OF CURRENT VARIATION OF LINEAR AND NON-LINEAR CIRCUITS

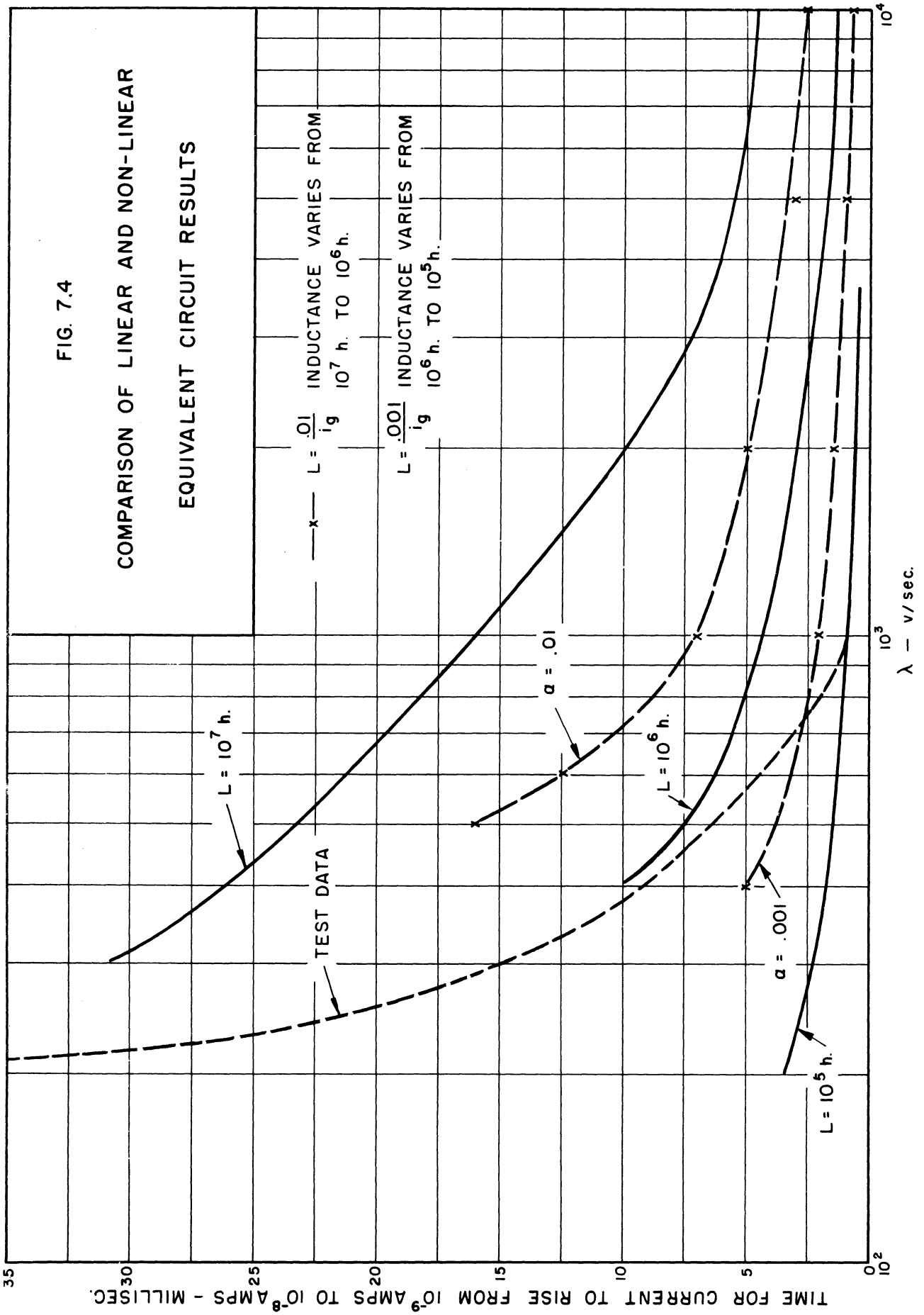
FIG. 7.4
COMPARISON OF LINEAR AND NON-LINEAR
EQUIVALENT CIRCUIT RESULTS
—x— L = .01/i_g INDUCTANCE VARIES FROM 10^7 h. TO 10^6 h.
L = .001/i_g INDUCTANCE VARIES FROM 10^6 h. TO 10^5 h.
L = 10^7 h.
TEST DATA
a = .01
L = 10^6 h.
a = .001
L = 10^5 h.
TIME FOR CURRENT TO RISE FROM 10^-9 AMPS TO 10^-8 AMPS - MILLISEC.
λ — v/sec.
35
30
25
20
15
10
5
0
10^2
10^3
10^4

and linear ($L = 10^6$ henries) examples, respectively. The time for the current to rise from i_o to i_f is shown to be $t = 16$ milliseconds and $t = 10$ milliseconds for the nonlinear and linear cases, respectively. These points are shown to be the end points of the $L = 10^6$ and $\alpha = 0.01$ curves shown in Fig. 7.4.

7.2 EFFECT OF CHANGING INITIAL AND FINAL CURRENT VALUES IN EQUIVALENT CIRCUIT

From the nonlinear data of Fig. 7.4 it can be seen that the experimental circuit operation is relatively poorly approximated by the equivalent circuit. Experimentally, the operating point i_o of the tube, on the grid-cathode static characteristic, has an important effect on the time it takes for the tube to fire with an applied linear rate of rise signal. With the operating point i_o near the breakdown current i_f of the tube, instability occurs as is to be expected, but shorter firing times also result, and conversely, with the operating point near or on the positive slope region of the static characteristics, stability is increased at the sacrifice of longer firing times. Since the values of α, i_o, and i_f used in Fig. 7.4 do not approximate the circuit's performance very well, the effects of changing the initial current and also the effects of extending the range of the firing current i_f were considered.

Figure 7.5 shows the results of a change in the initial current i_o. Also drawn on this graph is the experimental circuit characteristic obtained from the setup shown in Fig. 5.1 with the corresponding operating conditions. As expected, shorter time intervals result as the initial current approaches the critical value. Sharper curves also result from higher values of initial current. The "breakpoint" shown on the circuit characteristic is the point at which the time of firing ceases to occur after an exact time interval. For lower values of λ the experimental curve represents a statistical average of the firings, as noted earlier.

In Fig. 7.6 the effect of changing α to a lower value is shown for two values of initial current. Finally, in Fig. 7.7, the effect of changing the terminal current in the equivalent circuit is shown. Variations of these factors do not improve the correlation between analytical and experimental data at low λ.

7.3 INVESTIGATION OF OTHER NONLINEAR ELEMENTS

The adoption of the parameter $L = \alpha/i_g$ appears valid only for values of λ greater than 5×10^2 volts/sec. For lower λ there is a large deviation between experimental and equivalent circuit results. Since variation of the parameters α, i_o, and i_f in the equivalent circuit do not appear to improve the fit to any appreciable degree, it was decided to alter the nonlinear element in some manner in the hope that the experimental data would be simulated to a closer degree for the lower λ regions. Take, for example, the nonlinear case where $f(i_g) = \beta/i_g^2$.

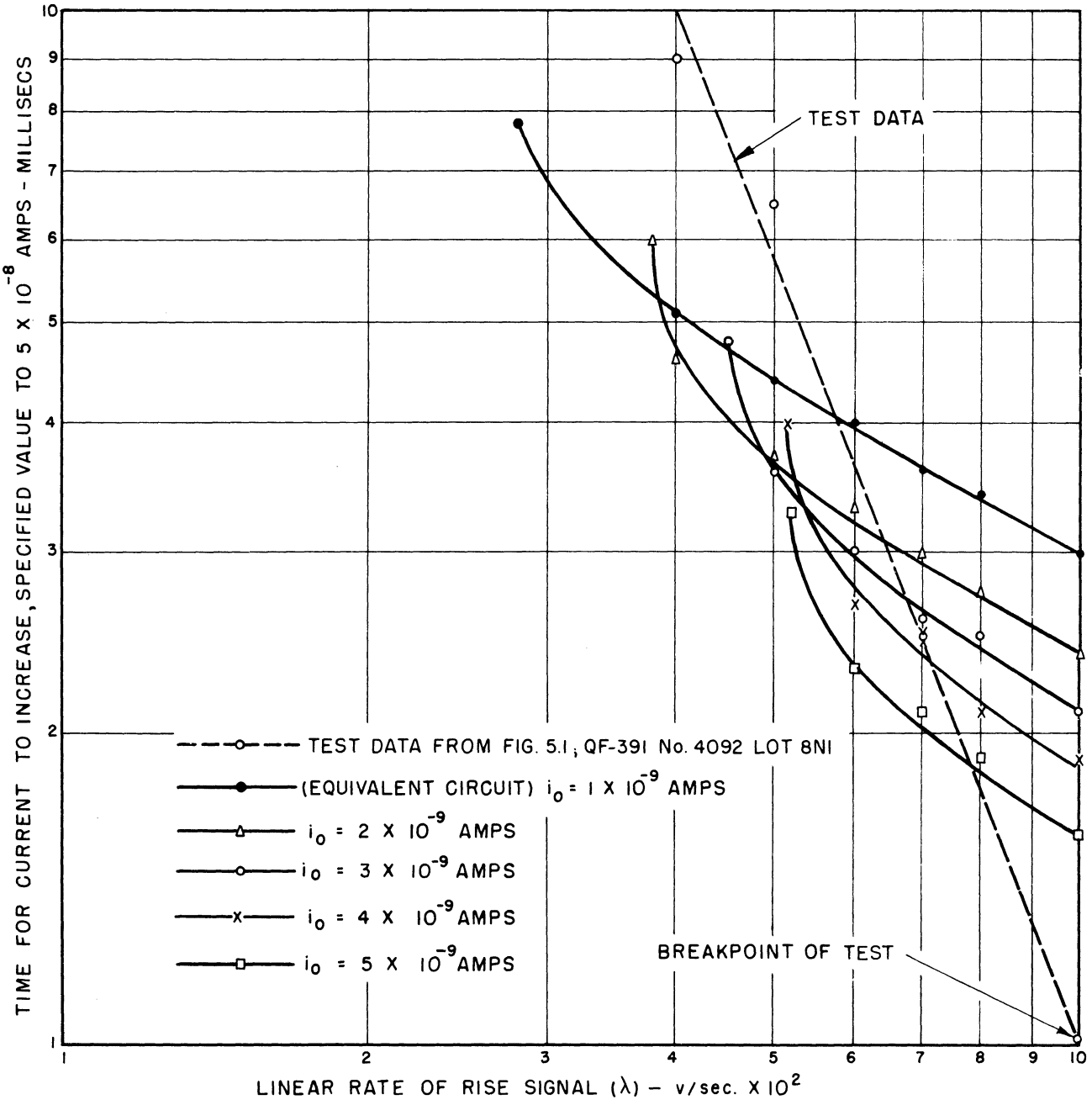

FIG. 7.5 RESULTS OF VARYING INITIAL CURRENT (i_0) IN NON-LINEAR EQUIVALENT CIRCUIT OF FIG. 7.1

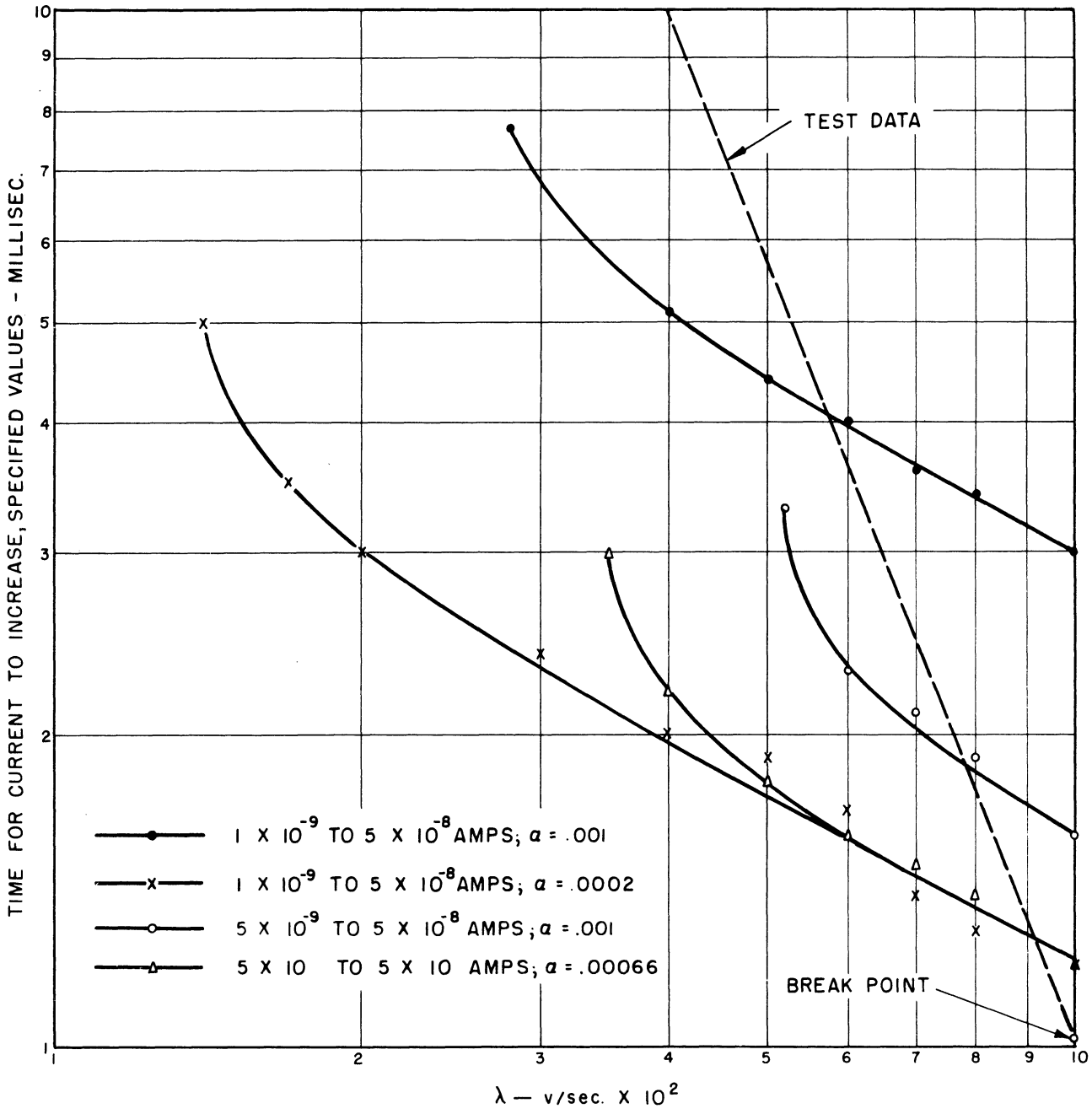

FIG. 7.6 RESULTS OF VARIATION OF α IN EQUIVALENT CIRCUIT

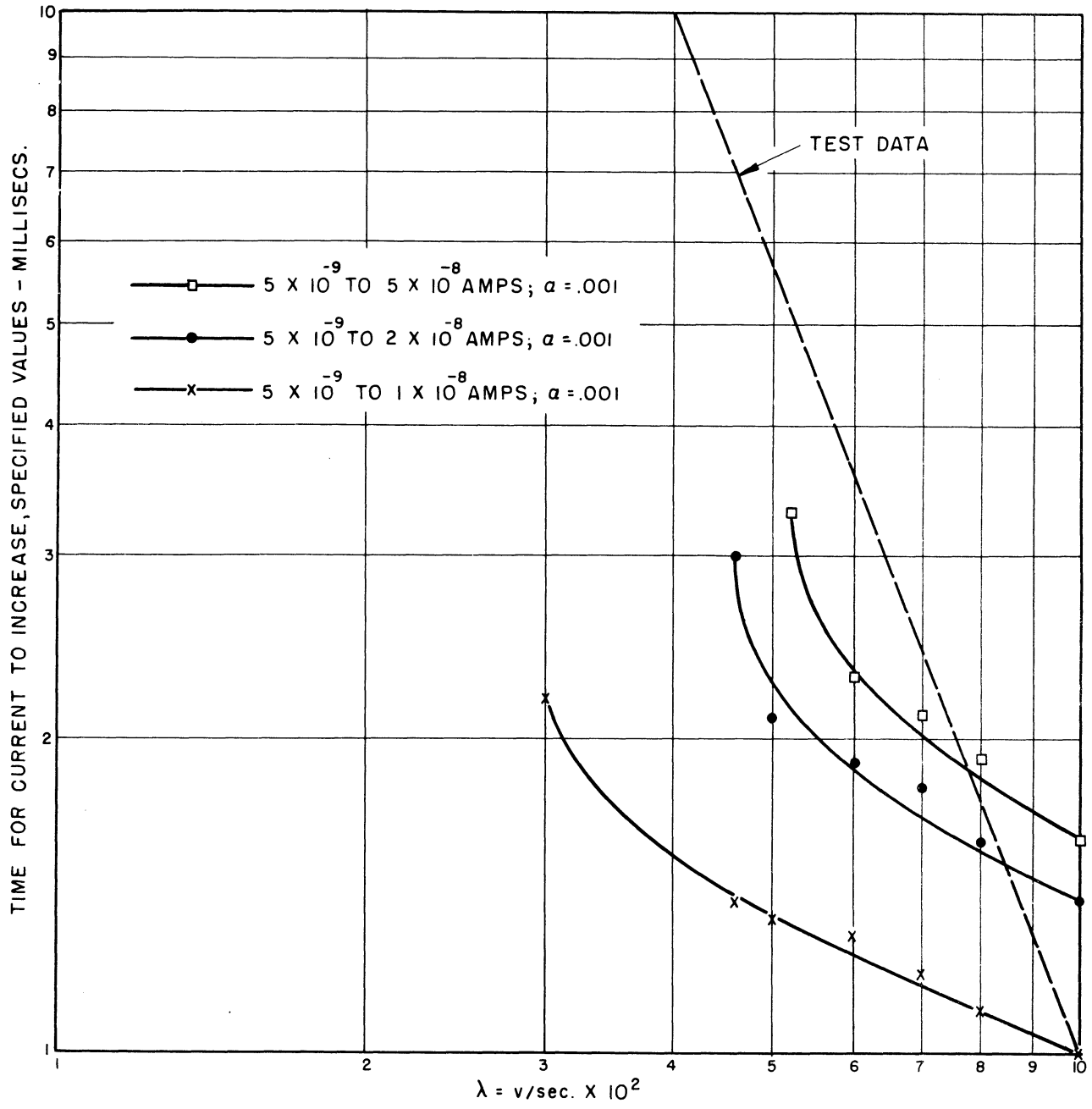

FIG. 7.7 RESULTS OF VARIATION IN FINAL CURRENT (i_o) IN THE EQUIVALENT CIRCUIT

Returning to the linear results of Fig. 5.1, it can be seen that the circuit characteristic values can be bounded to a closer degree for L = 10^7 henries and L = 10^5 henries. Therefore, the nonlinear element should vary from 10^7 to 10^5 henries in the lower regions of λ for a closer approximation to the experimental results. This means that the $f(i_g)$ coefficient in Eq. 7.1 should vary in the following manner:

$$f(i_g) = \frac{\beta}{i_g^2} = \frac{10^{-11}}{10^{-18} \text{ to } 10^{-16}} = 10^7 \text{ to } 10^5 \text{ henries} .$$

The result of using this function to simulate the time-lag mechanism of the tube is shown in Fig. 7.8. As can be seen, this nonlinear function seems to approximate the experimental data better in the low λ region. Since the correlation is still not as good as one might desire, a third nonlinear function can be tried. Thus consider the nonlinear case where $f(i_g) = \xi/i_g^3$.

In this case we let the function $f(i_g)$ vary from 10^8 to 10^5 henries.

$$f(i_g) = \frac{\xi}{i_g^3} = \frac{10^{-19}}{10^{-27} \text{ to } 10^{-24}} = 10^8 \text{ to } 10^5 \text{ henries} .$$

The results of employing this nonlinear function are shown to correlate a little closer for the low λ regions. Therefore it seems that, as the inverse power of i_g was increased in the $f(i_g)$ coefficient, the equivalent circuit data better approximate the experimental results.

Returning to the case employing the first power of i_g, the apparent poor simulation at low λ region is likely due to the fact that operation at low λ is not according to our conception.

The computer results of the equivalent circuit suggest that there is another effect present in test circuit operation aside from the statistical aspect common to breakdown phenomena. Thus it may be possible to augment the explanation by considering firing at some "later oscillation" than the first peak for lower values of λ. To substantiate this, the problem was considered in this respect as described in the next section.

8. INVESTIGATION OF OSCILLATIONS BY GROUP FIRING DATA

In this section the experimental λ-vs-t curves are considered in detail for evidence of oscillations occurring across the grid-cathode gap before breakdown for the low values of λ. The data in this section can be obtained by use of the setup shown in Fig. 5.1.

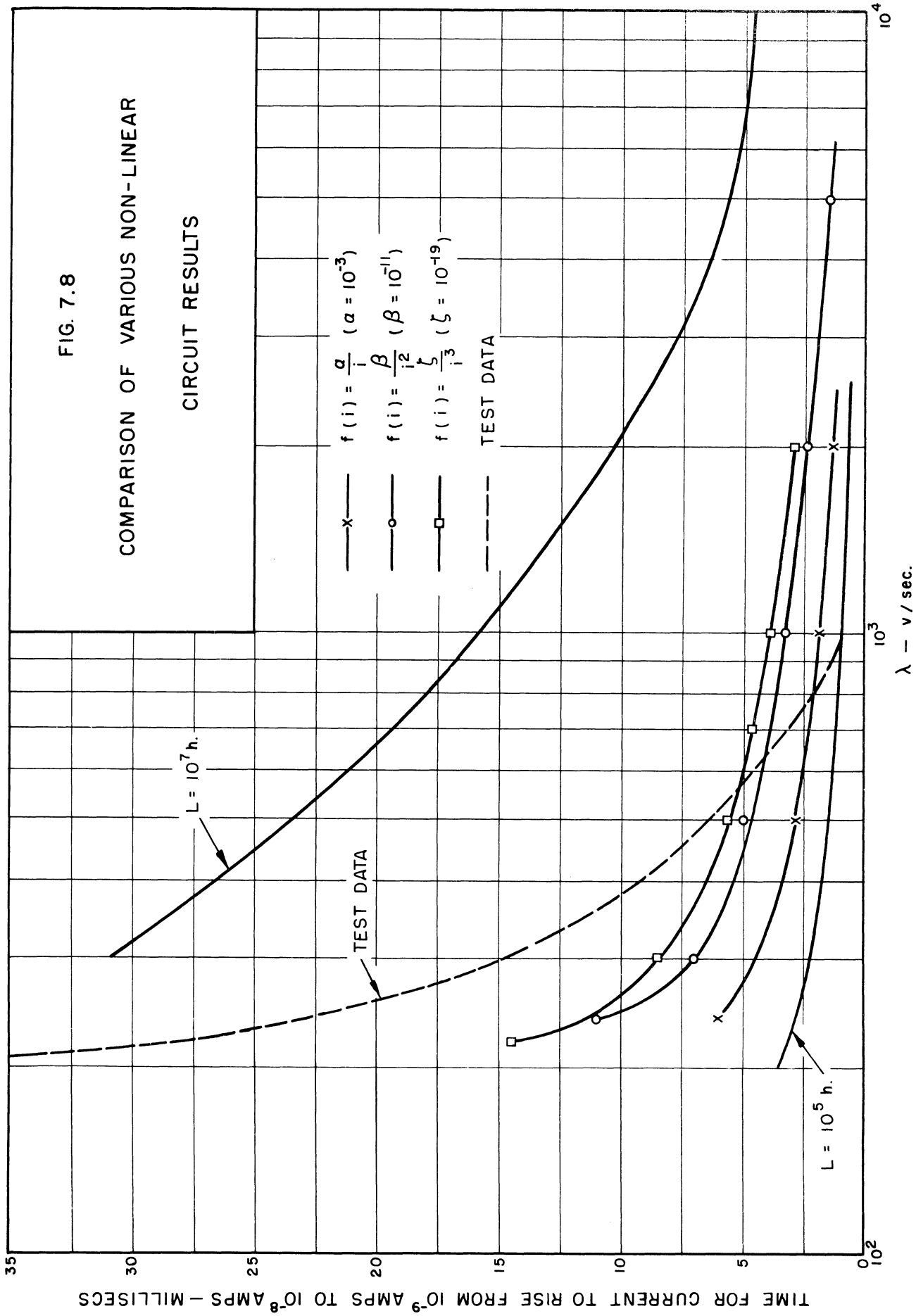
FIG. 7.8
COMPARISON OF VARIOUS NON-LINEAR
CIRCUIT RESULTS
f(i) = a/i (a = 10^-3)
f(i) = β/i^2 (β = 10^-11)
f(i) = ζ/i^3 (ζ = 10^-19)
TEST DATA
L = 10^7 h.
TEST DATA
L = 10^5 h.
λ — v / sec.
TIME FOR CURRENT TO RISE FROM 10^-9 AMPS TO 10^-8 AMPS — MILLISECS
35
30
25
20
15
10
5
0
10^4
10^3
10^2

Prior to this point, the experimental firing data of the circuit were considered a continuous λ-vs-t curve of the type shown on Fig. 5.2. For the higher values of λ, it was noted that the tube consistently fired at the same time for each particular value of λ. In that region the equivalent circuit is valid with respect to predicting the firing time interval for the circuit. However, as λ is decreased, it is noted that the firing times are no longer a unique function of λ but appear somewhat random in nature. Therefore, the continuous curve for values after the breakpoint of the gap represented an average picture of a wide scattering of points for each λ. It is also in this region that the equivalent circuit data deviate from the experimental data to a large degree. This deviation between the two sets of data can be explained as follows.

The wide scattering of firing times for low values of λ is attributed to the occurrence of current oscillations across the grid-cathode gap before breakdown. To substantiate the concept, many tube firings were conducted to obtain a quantity of data which would enable detection of the possibility of the tube firing after more than a particular time interval.

Figure 8.1 shows the results of firing a tube 100 times at a value of λ = 500 volts/sec and an initial operating current of $i_o = 2.4 \times 10^{-9}$ amp. At this value of λ there appears to be a 50-50 chance that the tube will fire during the second group or oscillation of grid current i_g. As can be seen from the graph, there is a distinct interval of time occurring between the groups. Therefore, if these groups are regarded as representative of a particular oscillation of grid current, then the approximate 5-millisecond time interval between groups represents a period of oscillation.

Returning to the data presented in Fig. 7.3 as representative of the current oscillation in the nonlinear equivalent circuit, it is seen that the oscillations are not equally spaced in regard to time as in the linear equivalent circuit. Therefore, it may be that the apparent inductance is not a nonlinear element depending on the instantaneous current i_g, but perhaps rather a constant which is dependent on the initial current i_o. This possibility will be considered later in the report.

From the data of Fig. 8.1, the frequency of oscillation is about 200 cps. These data represent a group firing for one value of λ and i_o. Other values of λ were tried with the same operating current i_o with the following results.

(1) When relatively high values of λ were applied ($\lambda > 10^3$ volts/sec), more than 95% of the firings occurred during the first group. This indicated that the firing times were occurring sometime during the rise of current on the first peak of oscillation. As λ was increased, the time interval between t = 0 and firing was shown to decrease. This meant that the firing current was reached nearer the beginning of the oscillation than before.

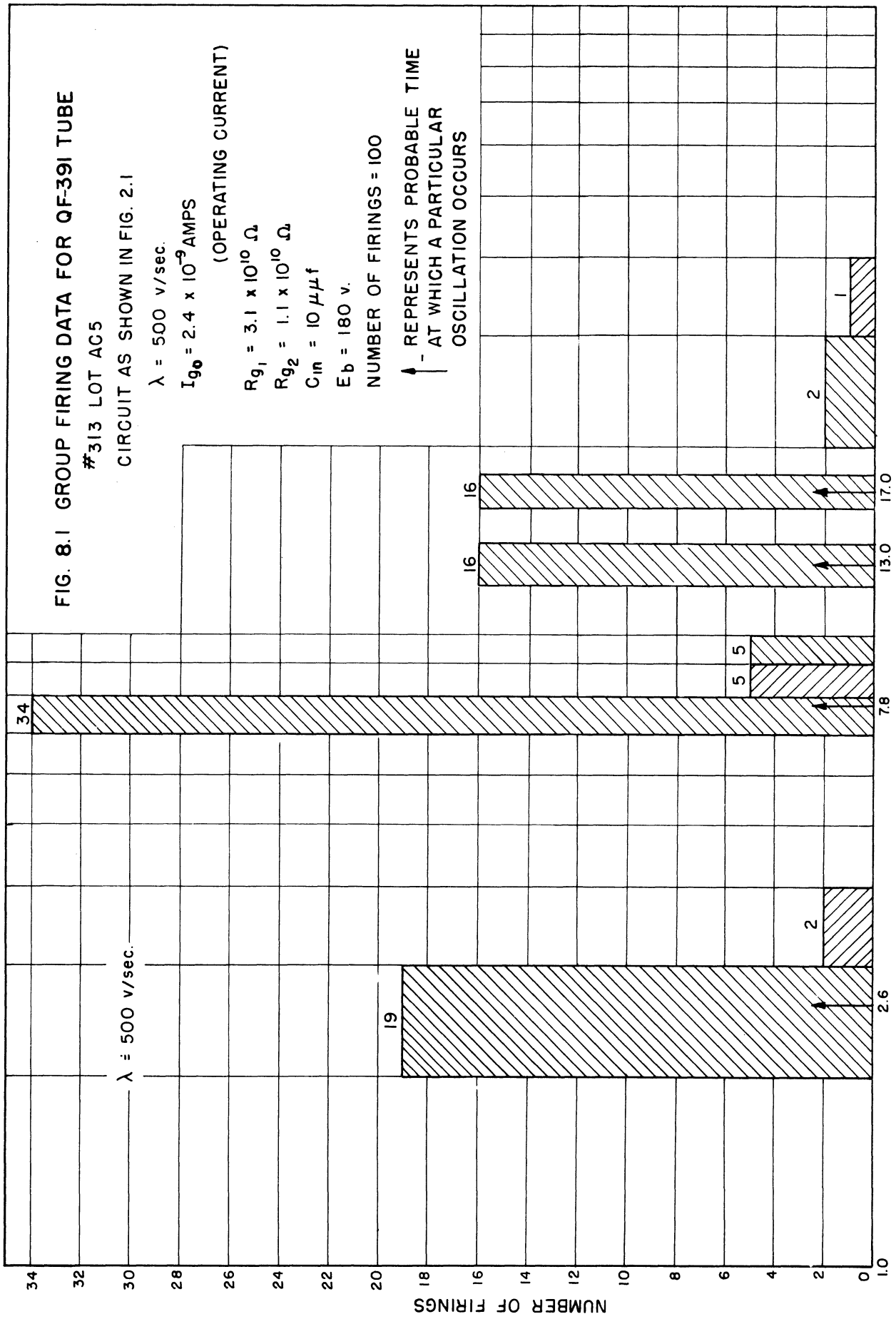
FIG. 8.1 GROUP FIRING DATA FOR QF-391 TUBE
#313 LOT AC5
CIRCUIT AS SHOWN IN FIG. 2.1
λ = 500 v/sec.
I_{g_0} = 2.4 x 10^{-9} AMPS
(OPERATING CURRENT)
R_{g_1} = 3.1 x 10^{10} Ω
R_{g_2} = 1.1 x 10^{10} Ω
C_{in} = 10 μμf
E_b = 180 v.
NUMBER OF FIRINGS = 100
REPRESENTS PROBABLE TIME AT WHICH A PARTICULAR OSCILLATION OCCURS
λ = 500 v/sec.
NUMBER OF FIRINGS
TIME OF FIRING - MILLISECONDS
34
19
2
5
5
16
16
2
1
1.0
2.6
7.8
13.0
17.0

(2) As λ was decreased to about λ = 800 volts/sec, the percentage of firings occurring during the first group dropped to 71. The percentage of firings in the second group increased slightly to 16. This shows that the probability of the tube firing on the second oscillation was increased as λ was decreased.

(3) At λ = 500 volts/sec, the percentage of firings occurring during the first group dropped to 21, while the second group increased to 44. Also at this low value of λ, evidence of a third and possibly a fourth group appeared. This further indicated that at very low values of λ, near the forbidden region, a number of current oscillations might occur before the grid-cathode breakdown current is reached. This apparently explains the sharp deviation between the analytical and experimental data at the low values of λ, for the analytical data were taken on the basis of the tube firing during the first oscillation for all λ. Therefore, if the analytical data from the equivalent circuit are to approximate the experimental data, the presence of the later oscillations must be considered.

(4) As λ was decreased further, the percentage of firings occurring in group one decreased rapidly, while the percentage of firings in groups three and four increased. Finally, at low λ ($\lambda < 350$ volts/sec), the tube ceased to fire.

(5) As the previous values of λ were varied and the grid-cathode characteristics remained constant, it was noted that the interval between all groups remained constant.

From the preceding information it is seen that the continuous type of λ-vs-t curve cannot be considered valid for representing accurately the time at which the tube may fire as a function of λ. In order that the oscillations can be represented by the λ-vs-t curves and thus give an acceptable representation of the circuit's dynamic performance, a curve of the form shown in Fig. 8.2 should be drawn. This type of presentation gives complete information regarding oscillations, from which we can construct a more accurate type of λ-vs-t curve. Then assuming that the current oscillation across the grid-cathode gap results from a constant inductance parameter as indicated by the experimental results, the λ-vs-t curves should be drawn in the following manner:

POINT (1)

Assume firing a tube a number of times at a relatively high value of λ. Of these firings, the greater percentage occur during the first group or oscillation, as indicated by the heavily cross-hatched bar at λ_4 as shown by Fig. 8.2. The time for firing of this predominant group is plotted as point (1) on the λ-vs-t graph shown in Fig. 8.4 where $\lambda_c = \lambda_4$ of Fig. 8.2.

Then assuming that the grid-cathode current can be represented as a sine wave of exponentially increasing amplitude, due presumably to the linear induc-

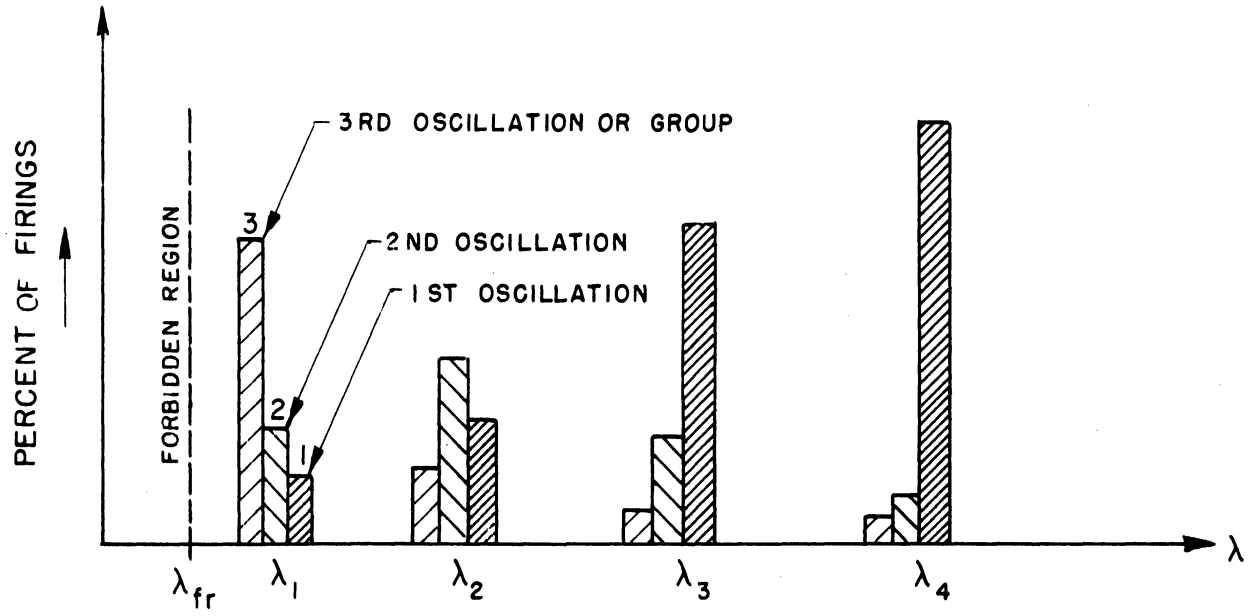

FIG. 8.2 GRAPH SHOWING PERCENT OF FIRINGS OCCURRING DURING VARIOUS GROUPS

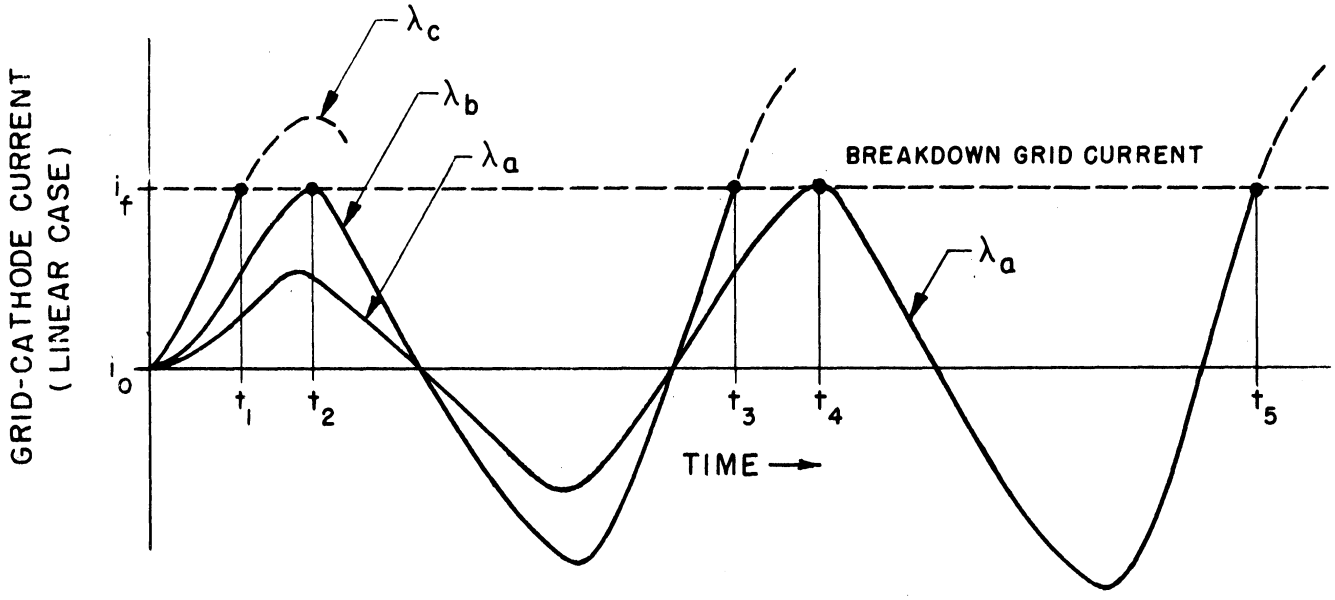

FIG. 8.3 CURRENT VARIATION OF GRID CIRCUIT ASSUMING LINEAR COMPONENTS

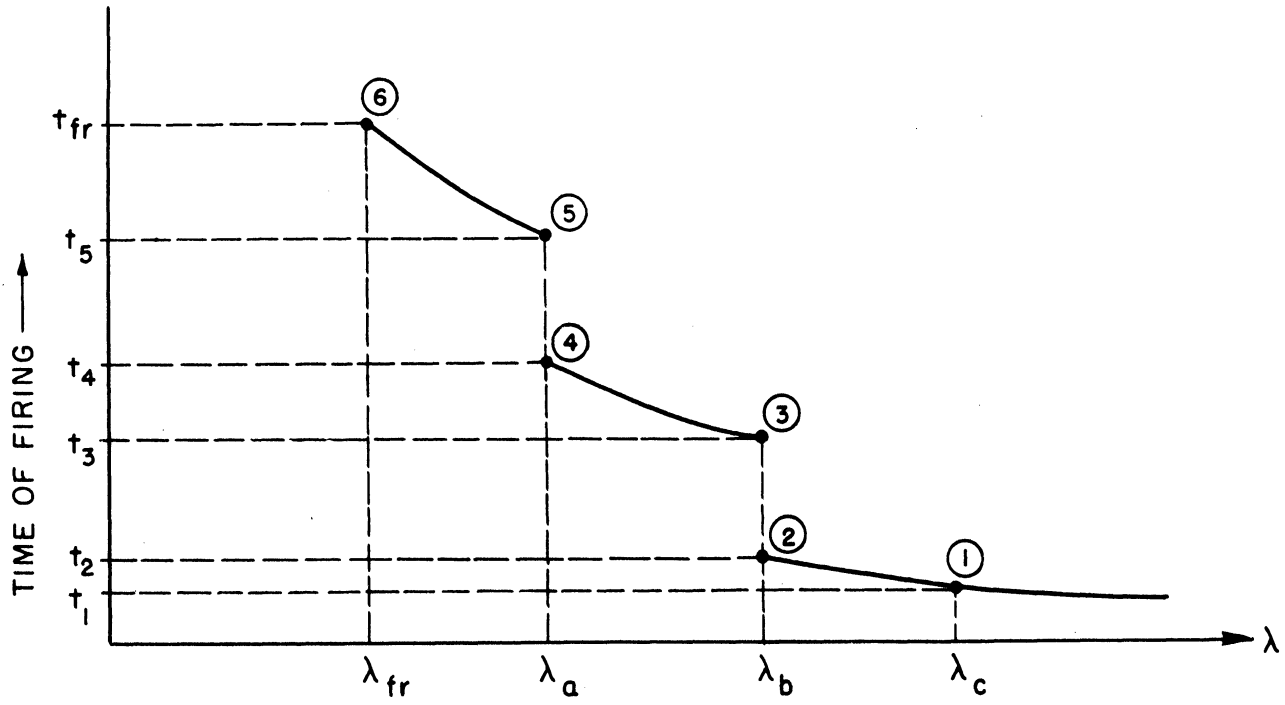

FIG. 8.4 λ VERSUS t CURVE

tance parameter, we can explain point (1) in the following manner. At t = 0 the grid-cathode current is at the bias value of i_o. After the application of the λt signal to the circuit, this current rises to a value depending on λ and the components in the circuit. Since the value $\lambda_c = \lambda_4$ is large enough to cause the current to increase to the value of grid-cathode breakdown current i_f, during the first oscillation the tube fires at some time t_1 as indicated in Fig. 8.3. However, as Fig. 8.2 shows, firing does not always occur during the first cycle. Thus one must consider that the curve labeled λ_c, Fig. 8.3, represents the most likely situation under the $\lambda = \lambda_4$ conditions. This seems a reasonable conclusion, for the curves drawn in Fig. 8.3 are only approximate representations of a largely statistical process.

POINTS (2) AND (3)

Now returning to Fig. 8.2, we find that at a value of λ, where $\lambda_3 > \lambda > \lambda_2$, groups one and two become almost equal in regard to percentage of firings. Therefore, to describe this point on the graph, we define this value of λ as equal to some λ_b. By knowing the times at which groups λ_2 and λ_3 appear, we locate the points (2) and (3) on the λ-vs-t curve.

Returning to the linear circuit assumption, we can describe these points in the following manner. At $\lambda = \lambda_b$ we find that this is just the value of input signal needed to drive the current to the value i_f on the first oscil-

lation. However, since it is so close that the current might not reach i_f for some reason on the first oscillation $t = t_2$, it would reach i_f sometime later on the second oscillation $t = t_3$. Therefore, since the tube fired 50% of the time on the first oscillation and 50% of the time on the second oscillation, we can represent these values of $\lambda = \lambda_b$ by points (2) and (3).

POINTS (3) AND (4)

In this range the percentage of firings during the second oscillation will prevail. The time at which this group occurred would be represented by time from t_3 to t_4.

POINTS (4) AND (5)

These points will represent the value of $\lambda = \lambda_a$ where 50% of the firings occur on the second oscillation and 50% on the third oscillation. These points are explained as points (2) and (3).

$$\lambda_1 < \lambda_a < \lambda_2$$

POINT (6)

At this value of λ, the grid-cathode gap ceases to break down. Values of λ less than λ_{fr} define the "forbidden region."

It is interesting to note that by assuming linear operation, Fig. 8.3 can be constructed from Fig. 8.4. Then, from the current wave form of Fig. 8.3, the values of inductance, resistance, and capacitance needed in a linear circuit to produce this wave form can be calculated. Therefore, by obtaining the experimental data in the form of Fig. 8.2, and then constructing Fig. 8.4, a linear circuit could be determined to duplicate the experimental results.

It is observed that the intervals occurring between group firings are constant. However, from the nonlinear equivalent circuit data shown in Fig. 7.3, the period between current peaks is not constant for the various values of λ. Moreover, the time between two successive oscillations is quite large with respect to the experimental observed effects. Therefore, the linear equivalent circuit's oscillations seemed to correlate with the experimental group firing data much more closely than the nonlinear circuit where $L = \alpha/i_g$.

To investigate this point further, additional data were obtained to illustrate the dependence upon the initial current i_o as well as λ. It was noted that the interval occurring between two successive groups decreases as the initial current i_o is increased, indicating that a relationship exists between the time of current buildup across the gap and the initial operating cur-

rent. Furthermore, since the period of oscillation, as indicated by the group intervals, changes with i_o, there exists a definite relationship between the initial current and the frequency of oscillatory current buildup in the gap. This suggests that the inductance element used to simulate the time lag of current buildup through the gap has a constant value dependent primarily on the magnitude of the initial operating current.

It was thought that since the time required to obtain the group firing data was excessive, some other means of investigating the oscillation phenomena would prove beneficial. From the standpoint of tube life, an experimental setup which would require fewer firings would also be desirable. Thus, in view of the relationship which seemed apparent between the period of oscillation and the operating current i_o, we were led to try to investigate these oscillations by observing some resonance phenomena.

9. GRID-CATHODE RESONANCE EFFECT AS A FUNCTION OF THE INITIAL OPERATING CURRENT i_o

In the preceding section, it was noted that the time interval between group firings is a function of the initial grid-cathode current i_o, denoting that the frequency of oscillation of the grid-cathode current i_g is a function of i_o. Then since the time interval between any of the groups for a particular λ seems constant, this dependence further suggests that the inductance parameter has a constant value whose magnitude is a function of the initial current i_o, rather than a nonlinear inductance whose value varies with the instantaneous values of grid-cathode current i_g.

To investigate this dependence, an experimental procedure was adopted using an alternating input signal for the driving voltage instead of the λt-signal. The resonant frequency of oscillation for various operating currents i_o could then be determined directly by noting at what input frequency the tube becomes most sensitive.

The setup shown in Fig. 9.1 was used, and the initial operating conditions were adjusted equivalent to those of Fig. 8.1. The rms alternating voltage e_a was then applied to the grid circuit as shown, and the frequency increased from some low value until the tube fired, the firing determined by a signal appearing across R_x. Further increase in frequency resulted in continuous firing of the tube, but finally, at a still higher frequency, the tube ceased firing. The alternating voltage e_a was then decreased and the procedure repeated. The result of this type of experimentation for the same tube and operating conditions of Fig. 8.1 is shown in Fig. 9.2. A distinct resonance occurs at about 200 cps, which is the frequency of oscillation calculated from Fig. 8.1 for this particular value of i_o. Thus, the resonant frequency of the grid circuit found by group firings and by applying an alternating voltage to the grid circuit correspond. Figures 9.3 and 9.4 illustrate the dependence of the apparent resonant frequency on the initial current.

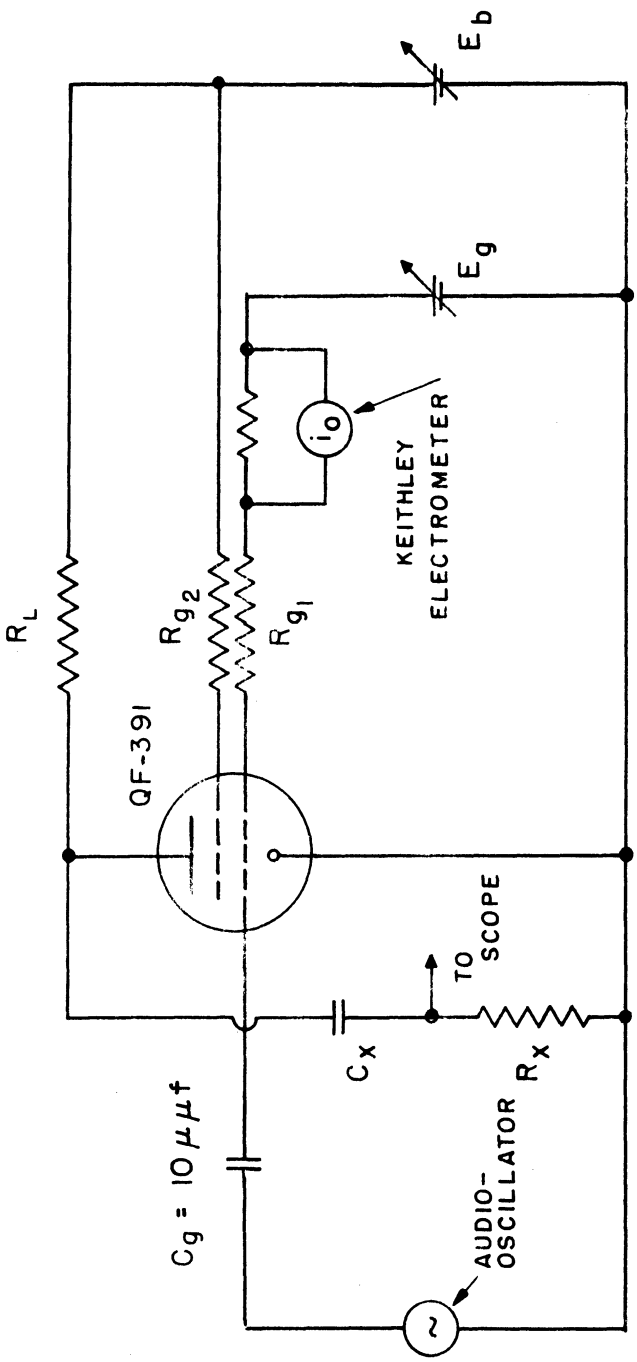

FIG. 9.1 SETUP FOR INVESTIGATING GRID-CATHODE RESONANCE

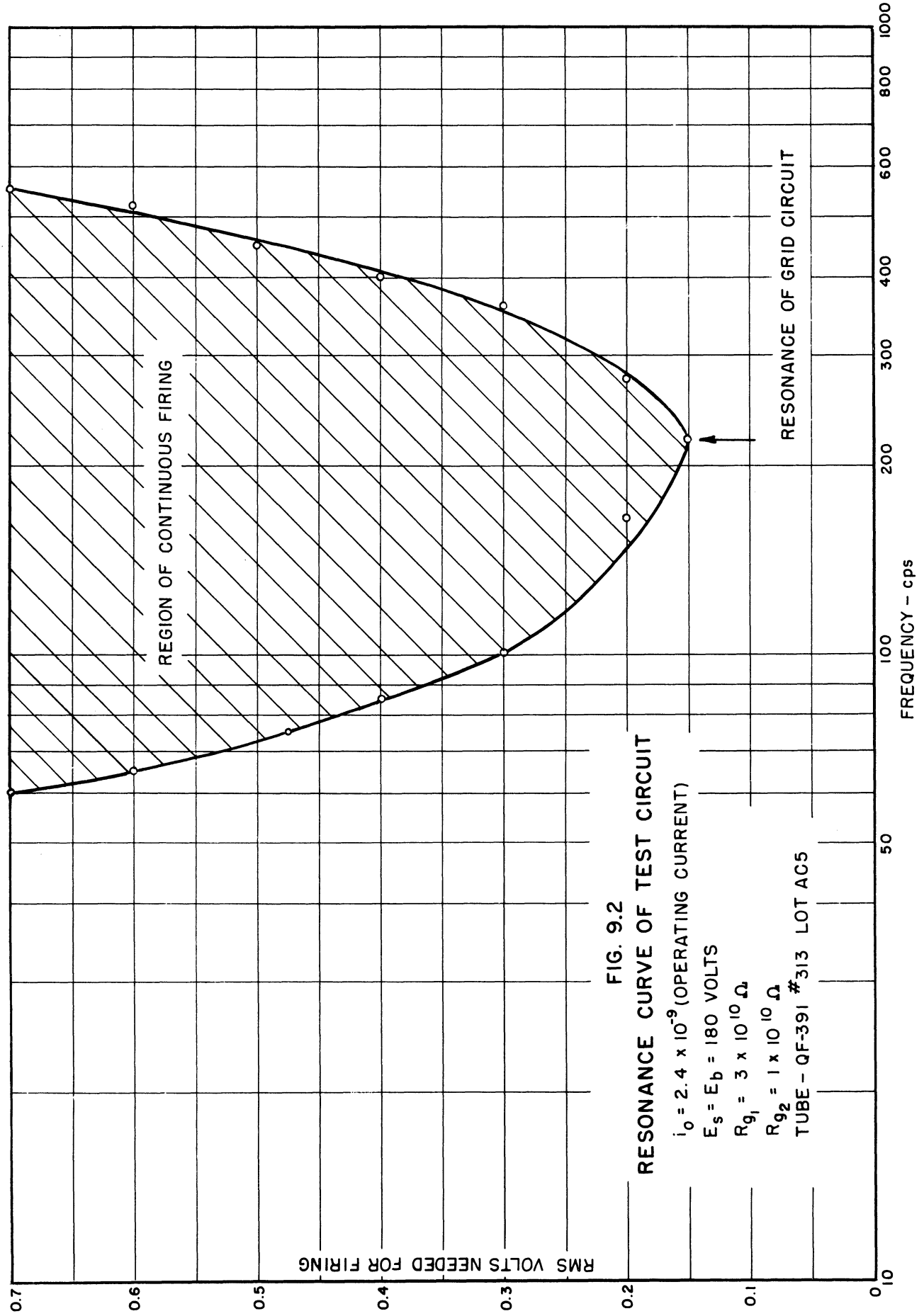

FIG. 9.2
RESONANCE CURVE OF TEST CIRCUIT
$i_o = 2.4 \times 10^{-9}$ (OPERATING CURRENT)
$E_s = E_b = 180$ VOLTS
$R_{g_1} = 3 \times 10^{10}\ \Omega$
$R_{g_2} = 1 \times 10^{10}\ \Omega$
TUBE – QF-391 #313 LOT AC5

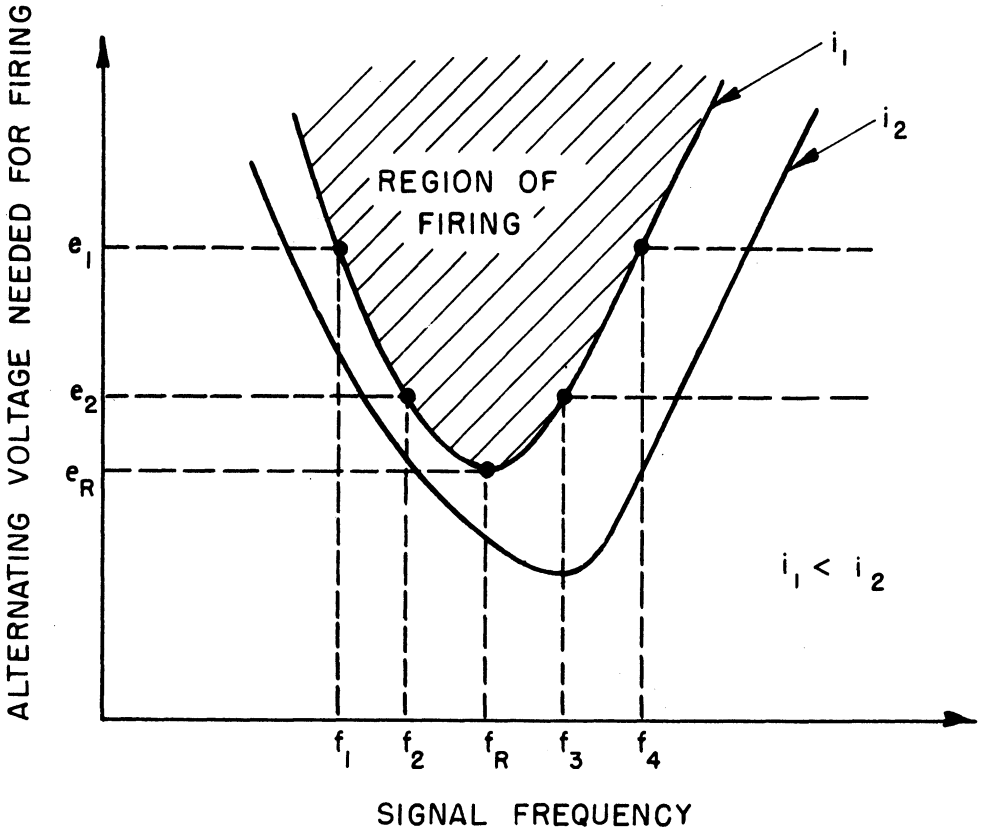

FIG. 9.3 TYPICAL RESONANCE CURVES FOR OPERATING CURRENTS i_1 AND i_2

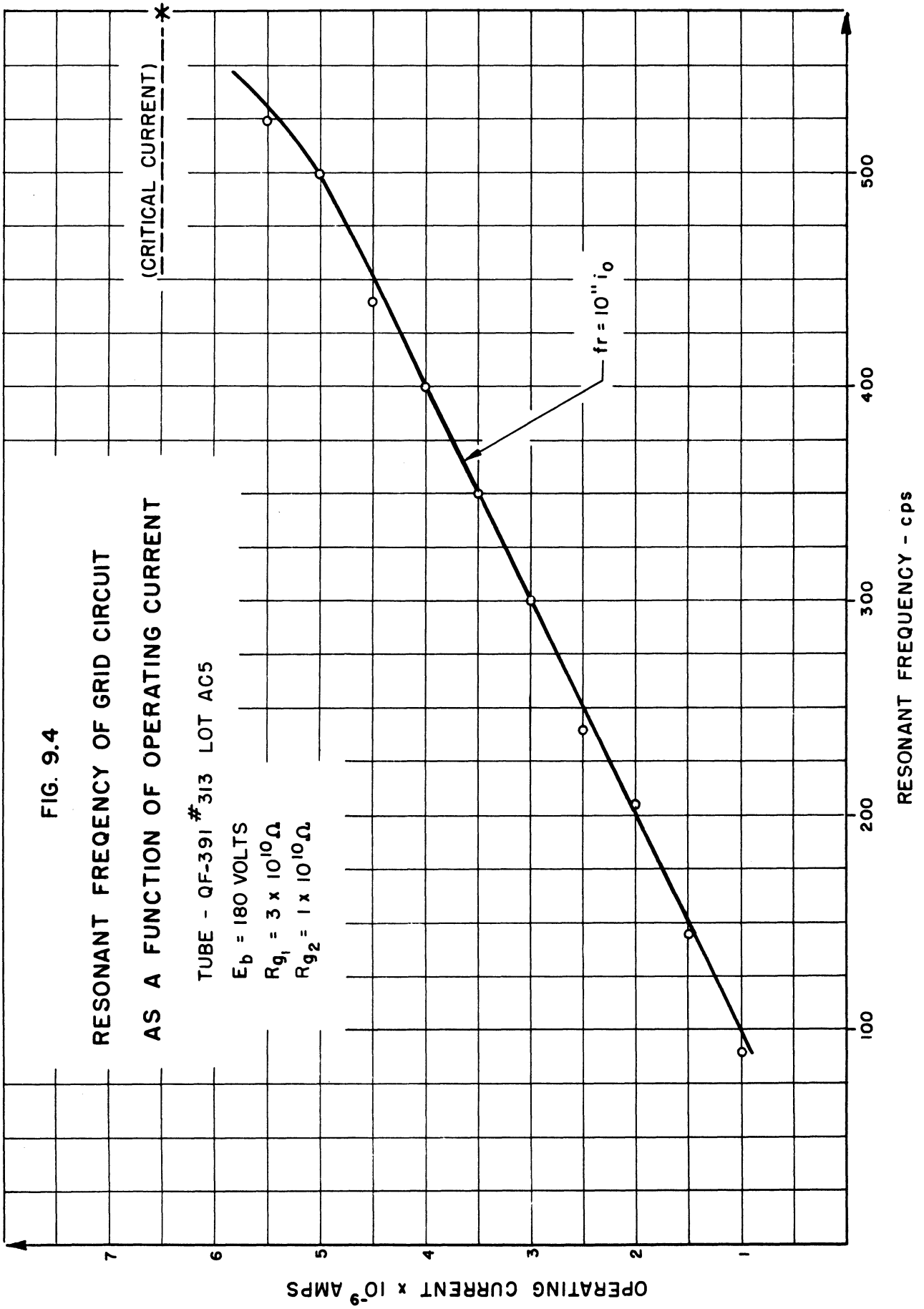
FIG. 9.4
RESONANT FREQENCY OF GRID CIRCUIT
AS A FUNCTION OF OPERATING CURRENT
TUBE - QF-391 #313 LOT AC5
E_b = 180 VOLTS
R_{g_1} = 3 x $10^{10}\Omega$
R_{g_2} = 1 x $10^{10}\Omega$
(CRITICAL CURRENT)
fr = 10'' i_o
OPERATING CURRENT x 10^{-9} AMPS
RESONANT FREQUENCY - cps
1
2
3
4
5
6
7
100
200
300
400
500

10. GRID-CATHODE RESONANCE DUE TO SHUNT CAPACITY C_{gc}

The interesting resonant effect discussed in the preceding section is clearly representative of the total equivalent circuit as illustrated in Fig. 9.2.

To obtain more information concerning the grid-cathode resonance of the tube, as contrasted with tube plus circuit, a revised setup eliminating the capacitor C_g was used, as shown in Fig. 10.1, and the corresponding (Fig. 10.2) equivalent circuit. With this setup, the resonance effect seems to be due only to the grid-to-cathode capacitance, 1.5 mmfd, the stray capacitance, and the inductance effect of the tube. Since the resistance shunting the Keithley electrometer and the 10^9 ohms are in series with the audio oscillator, the sensitivity of the system is not as high. However, our interest lies in the resonance phenomena of the gap and the sensitivity.

E_g was adjusted until the grid-cathode gap was operating at some initial current i_o, a value chosen to keep the tube operating on the negative slope of its static characteristic (see Appendix IV for characteristic). Resonance data were then obtained following the procedure of Section 9.

Figure 10.3 shows three somewhat irregular resonance curves obtained for different values of operating current. Curves at other values of current were also taken, but for the sake of clarity only three are shown here. It is noted that there appear two distinct resonance points for large values of operating current i_o, and that the frequency is much higher than that found from the previous setup (Fig. 9.2). Circuitwise, the only change is substitution of the series-connected Keithley for the C_g = 10 mm capacitor, and addition of the 10^9-ohm resistor.

Insufficient time prevented justification of the magnitude of the frequency change and the reason for a double-peaked curve. It is clear that the effective capacitance in the circuit was reduced by the above circuit change, which is consistent with the frequency increase. However, it is not apparent why the capacitance change should be the factor of 100 required for a factor of 10 frequency increase.

The presence of the 10^9-ohm resistors seems to have the effect of isolating the Keithley input capacitance ($\sim$ 6 mm) from the grid, for the capacitance reactance is a factor of 100 less than the series resistance.

Leaving this point unresolved, the assumption is made that the only effective capacitance in the grid circuit is the C_{gc} = 1.5 mmfd, and that the resonance effect observed involved the gap inductance.

Figure 10.4 illustrates the dependence of frequency upon initial

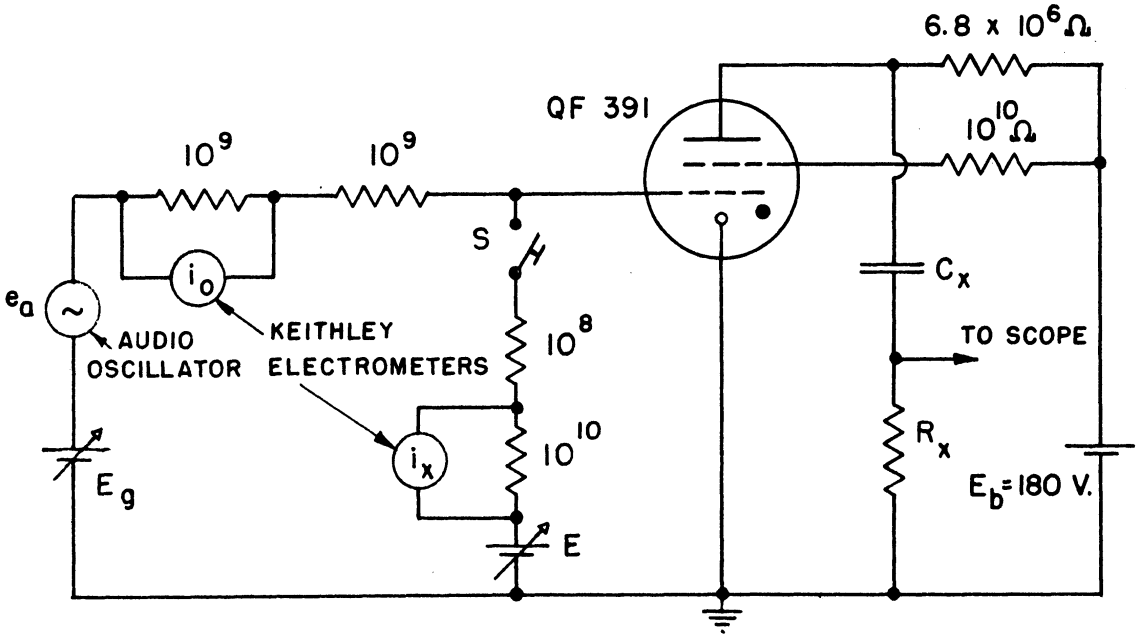

FIG. 10.1 SETUP FOR INVESTIGATING GRID RESONANCE

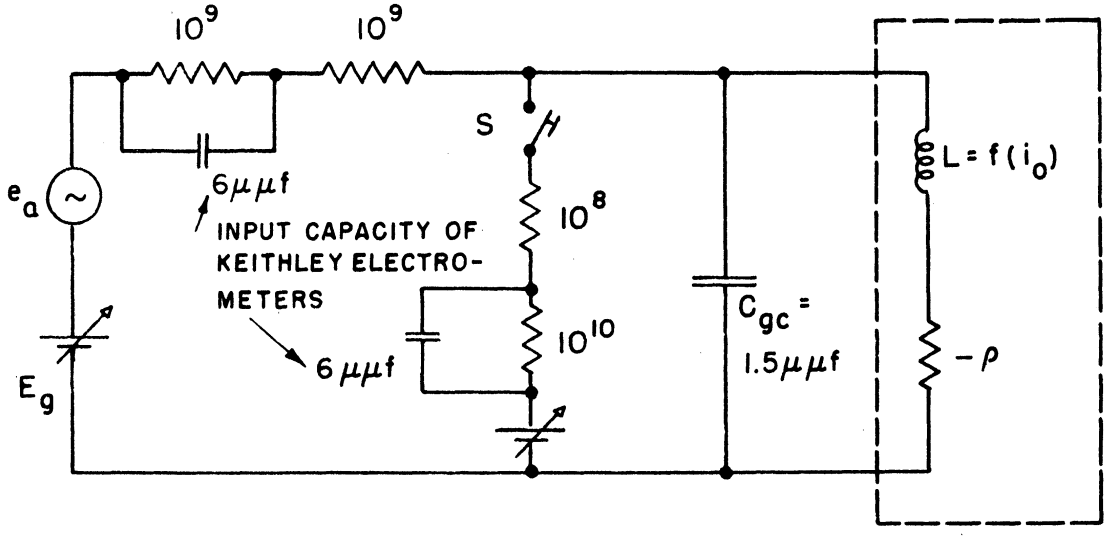

FIG. 10.2 GRID-TO-CATHODE DYNAMIC CIRCUIT

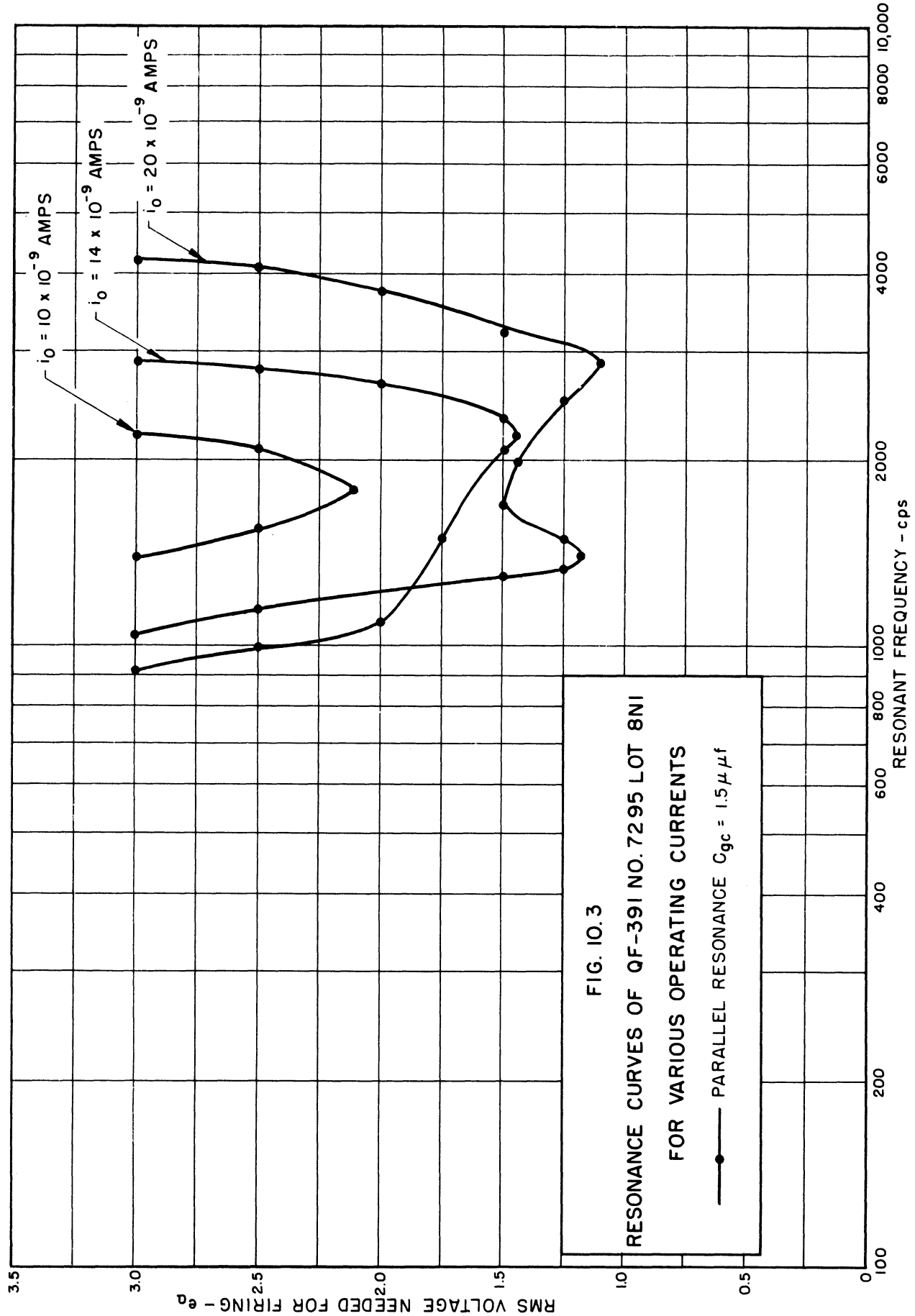
i_o = 10 x 10^{-9} AMPS
i_o = 14 x 10^{-9} AMPS
i_o = 20 x 10^{-9} AMPS
RMS VOLTAGE NEEDED FOR FIRING - e_g
RESONANT FREQUENCY - cps
3.5
3.0
2.5
2.0
1.5
1.0
0.5
0
100
200
400
600
800
1000
2000
4000
6000
8000
10,000
FIG. 10.3
RESONANCE CURVES OF QF-391 NO. 7295 LOT 8NI
FOR VARIOUS OPERATING CURRENTS
PARALLEL RESONANCE C_{gc} = 1.5 μf

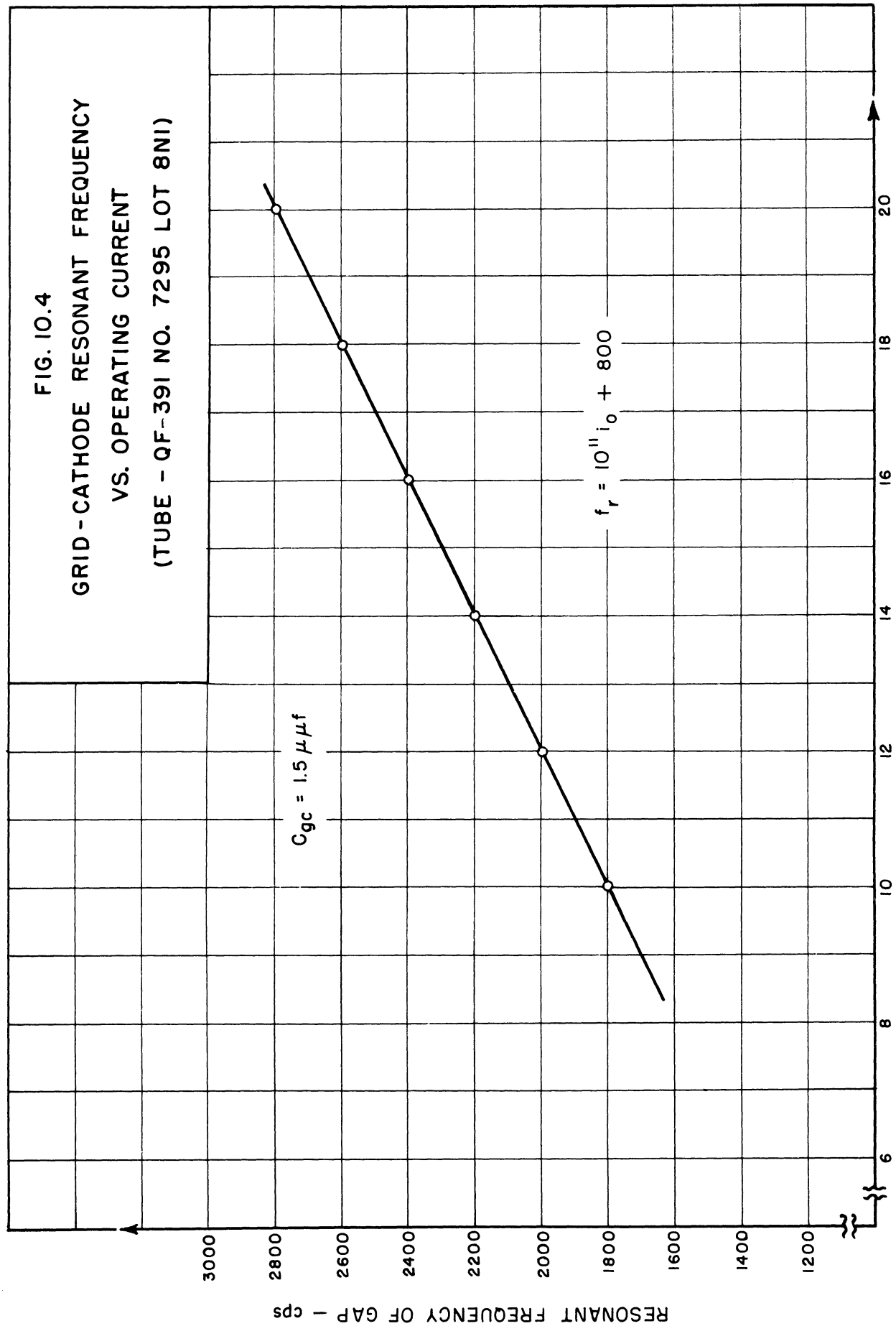
FIG. 10.4
GRID-CATHODE RESONANT FREQUENCY
VS. OPERATING CURRENT
(TUBE - QF-391 NO. 7295 LOT 8NI)
C_{gc} = 1.5 $\mu\mu$f
$f_r = 10^{11} i_o + 800$
RESONANT FREQUENCY OF GAP - cps
3000
2800
2600
2400
2200
2000
1800
1600
1400
1200
OPERATING CURRENT - (i_o X 10^{-9} AMPS)
6
8
10
12
14
16
18
20

current. From the curve:

$$f_r = 10^{11} i_o + 800 \quad . \tag{10.1}$$

On the basis of the assumption made above, in regard to C_{gc}, a relationship can be written:

$$f_r = 10^{11} i_o + 800 = \frac{1}{2\pi \sqrt{L_g C_{gc}}} \tag{10.2}$$

11. CONCLUSIONS AND SUMMARY

As a result of this research work and the preparation of this report, several conclusions seem clear, although additional investigations should be carried out to establish firmly their validity and to "fill in" some missing details.

1. The delays observed in firing of a small gap under the influence of an applied signal, such as a ramp-function voltage, can be reasonably accurately simulated with an equivalent circuit which employs capacitance, inductance, and negative resistance. The nature of the inductance is not completely clear, but present indications are that it should be essentially constant, and of a magnitude determined by the initial Townsend current flowing in the gas.

2. The desired observations (employing an equivalent circuit) can best be made using an analog computer, which facilitates simulation of the negative resistance. Normally encountered minor variations of the computer elements seem to contribute to simulation of the statistical "firing effect" which is observed with the test circuit employing the tube.

3. The nature of the current buildup in the gap is oscillatory, and although satisfactory prediction of the frequency has not been realized, it appears to be predicted by the static capacitances of the circuit and the inductance mentioned in (1) above.

4. Static characteristics of subminiature tubes employing currents in the millimicroampere range can be readily and satisfactorily determined by the techniques employed in the course of this research program.

APPENDICES

APPENDIX I

ANALYTICAL SOLUTION OF A SERIES CIRCUIT EMPLOYING A NONLINEAR INDUCTANCE AND A NEGATIVE RESISTANCE

It is noted from investigating the nonlinear equation shown in Section 4 that a similar circuit omitting the capacitance can be solved analytically.

The following is a solution of the circuit shown in Fig. A-I-1. The circuit equation is

$$\left(\frac{\alpha}{i}\right)\frac{di}{dt} - Ri = E \quad . \tag{A-I-1}$$

Rearranging Eq. A-I-1, we obtain:

$$\frac{di}{dt} - \frac{R}{\alpha} i^2 = \frac{E}{\alpha} i \tag{A-I-2}$$

$$\int_{i_o}^{i} \frac{di}{i(Ri+E)} = \int_{o}^{t} \frac{dt}{\alpha} \tag{A-I-3}$$

$$\frac{1}{E} \ell n \frac{i}{Ri+E} - \frac{1}{E} \ell n \frac{i_o}{Ri_o+E} = \frac{t}{\alpha} \tag{A-I-4}$$

$$e^{\frac{Et}{\alpha}} = \frac{R + \frac{E}{i_o}}{R + \frac{E}{i}} \quad . \tag{A-I-5}$$

Finally Eq. A-I-5 can be solved for i.

$$i = \frac{i_o e^{\frac{Et}{\alpha}}}{1 - \frac{R}{E} i_o (e^{\frac{Et}{\alpha}} - 1)} \quad . \tag{A-I-6}$$

Using the values of the parameters as

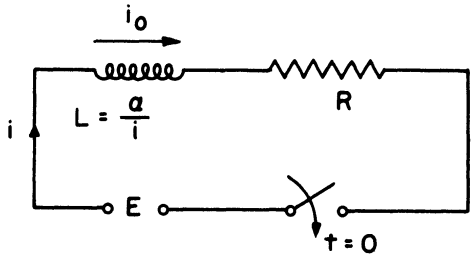

FIG.A-I-1 CIRCUIT CONTAINING NON-LINEAR INDUCTANCE AND NEGATIVE RESISTANCE

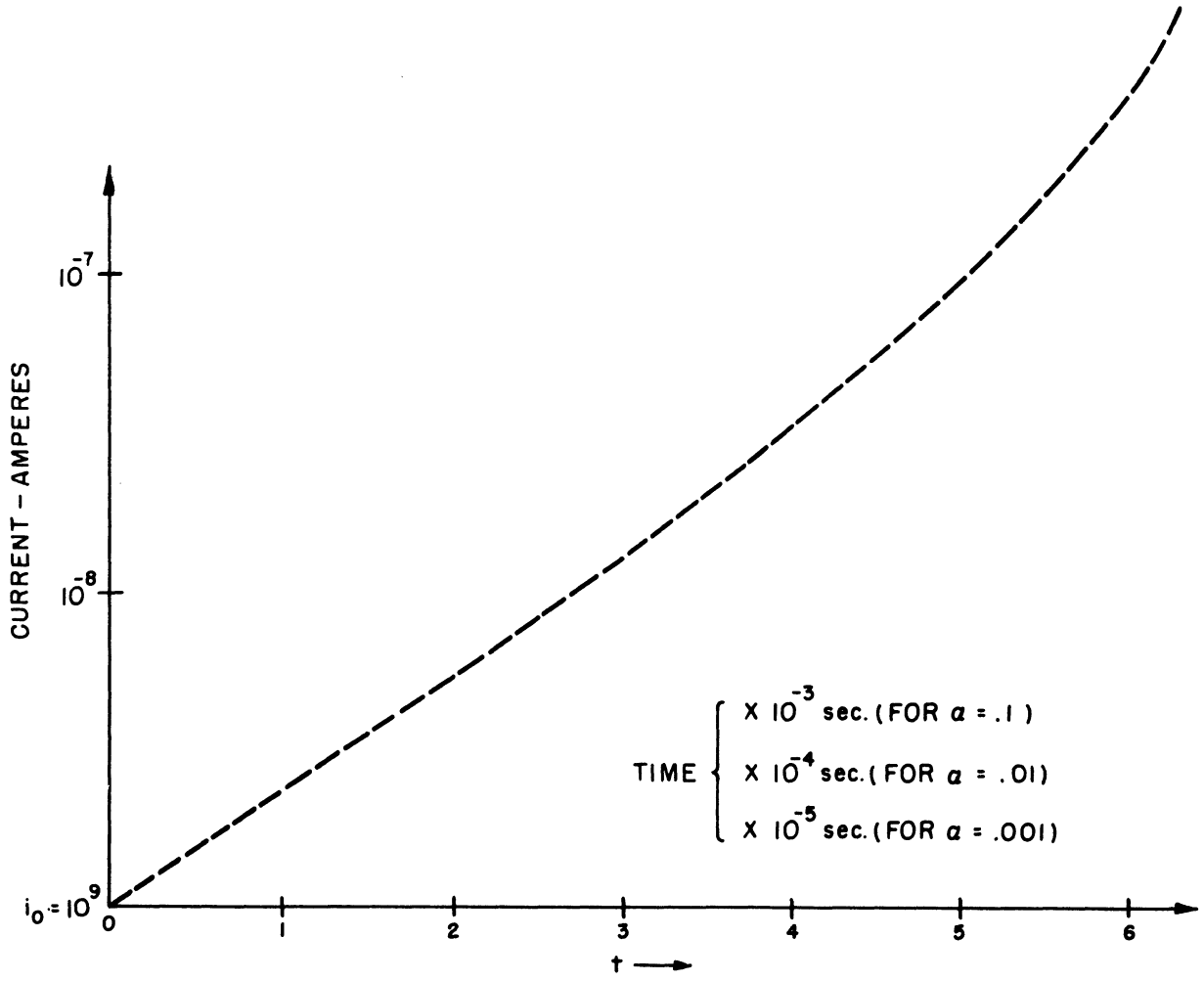

FIG.A-I-2 CURRENT VS. TIME FOR VARIOUS VALUES OF α

$L = \alpha/i$,

$\alpha = .1, .01, .001$,

$R = -10^8\ \Omega$,

$E = 100$ volts, and

$i_o = 10^{-9}$ amp (initial condition at $t = 0$).

From the denominator of Eq. A-I-6, it can be seen that i goes to infinity when

$$\frac{R}{E} i_o \left(e^{\frac{Et}{\alpha}} - 1\right) = 1 \quad . \tag{A-I-7}$$

For the values of the parameters given in the circuit, the time for the current to reach infinity is

$$t = 0.0691 \text{ sec} \quad . \tag{A-I-8}$$

The results of Eq. A-I-6 are plotted on Fig. A-I-2.

APPENDIX II

GRAPHICAL METHOD OF SOLVING A NONLINEAR DIFFERENTIAL EQUATION

In Section 4 the equation which described the current variation in the equivalent circuit is nonlinear, and a solution was not determined by ordinary analytical means. However, it was found that it could be solved by the following graphical technique, which is referred to as the phase-plane method. To illustrate it, we will consider the equation describing the test equivalent circuit.

$$\frac{R}{E} i_o \left(e^{\frac{Et}{\alpha}} - 1\right) = 1 \quad . \tag{A-II-1}$$

We now let

$$\alpha = 0.001,$$

$$R = -10^8\ \Omega,$$

$$C = 10^{-11} \text{ farads},$$

$$i = 10^{-9}\ I,$$

$$t = 10^{-3}\ T, \text{ and}$$

$$\lambda = 10^3 \text{ volts/sec}.$$

Substituting these values, Eq. A-II-1 becomes

$$\frac{1}{I}\frac{dI}{dT} - 10^{-1}\ I + 10^{-1} \int I dT = T \quad . \tag{A-II-2}$$

To solve Eq. A-II-2 by the phase-plane method, we first differentiate with respect to T to eliminate the integral term and the T term on the right-hand side of the equation.

$$\frac{1}{I}\frac{d^2I}{dT^2} - \frac{1}{I^2}\left(\frac{dI}{dT}\right)^2 - 10^{-1}\frac{dI}{dT} + 10^{-1}\ I = 1 \quad . \tag{A-II-3}$$

Any nth-order differential equation can be written as n separate first-order differential equations. For example:

$$\alpha_n \frac{d^n y}{dx^n} \cdots \alpha_3 \frac{d^3 y}{dx^3} + \alpha_2 \frac{d^2 y}{dx^2} + \alpha_1 \frac{dy}{dx} + \alpha_0 y = 0 \quad . \qquad \text{(A-II-4)}$$

Let

$$v = \frac{dy}{dx}$$

$$z = \frac{dv}{dx}$$

$$w = \frac{dz}{dx} \text{ , and } n = 2$$

etc.

$$\alpha_2 \frac{d^2 y}{dx^2} \alpha_1 \frac{dy}{dx} \alpha_0 y = 0 \quad . \qquad \text{(A-II-5)}$$

or

$$\alpha_2 \frac{dv}{dx} + \alpha_1 v + \alpha_0 y = 0 \qquad \text{(A-II-6)}$$

$$\frac{dv}{dx} = -\frac{\alpha_1}{\alpha_2} v - \frac{\alpha_0}{\alpha_2} y = 0 \quad . \qquad \text{(A-II-7)}$$

Thus Eq. A-II-5 can be represented by the two first-order differential equations (A-II-6 and A-II-8).

Therefore, returning to Eq. A-II-3 and letting

$$V = \frac{dI}{dT} \quad , \qquad \text{(A-II-8)}$$

we get

$$\frac{1}{I} \frac{dV}{dT} - \frac{V^2}{I^2} - 10^{-1} V + 10^{-1} I = 1 \quad . \qquad \text{(A-II-9)}$$

Then since

$$\frac{dV}{dI} = \frac{dV/dT}{dI/dT} \cdot \frac{dI}{dT} = \frac{dV}{dI} V \quad , \qquad \text{(A-II-10)}$$

we can now substitute Eq. A-II-10 into Eq. A-II-9 and eliminate the independent variable (T).

$$\frac{V}{I}\frac{dV}{dI} - \frac{V^2}{I^2} - 10^{-1} V + 10^{-1} I = 1 \quad . \qquad \text{(A-II-11)}$$

Rearranging Eq. A-II-11, we have

$$\frac{dV}{dI} = \frac{V}{I} + 10^{-1} I - \frac{10^{-1} I^2}{V} + \frac{I}{V} \quad . \qquad \text{(A-II-12)}$$

Equation A-II-12 is a differential equation involving only the current and the rate of change of current, independent of time. When the initial values of V and I are known from the initial conditions of the original equation, the dV/dI term can be computed. The value of this term (slope) is then plotted (see Fig. A-II-1) on a graph of V vs I. Through some point I_1V_1 which this line intersects, another value of dV/dI again is computed from the new values of i_1 and V_1. This process is continued until a so-called phase-plane curve of V vs I is finally drawn. The accuracy of this plot is determined by the interval chosen between successive points of calculation; the smaller this interval, the greater the accuracy.

After establishing a phase-plane plot of the solution of Eq. A-II-12, the next step is to find the value of T for each value of current I and rate of change of current V.

From Eq. A-II-8 we get

$$T = \int_{I_o}^{I} \frac{1}{V}\, dI \quad . \qquad \text{(A-II-13)}$$

Therefore, the time interval from I_o to I is represented by the area under the 1/V-vs-I curve between these two values of I. By finding enough values of time for different values of current, we finally obtain the current-vs-time curve which is the solution to Eq. A-II-3.

Since we are interested only in finding the time it takes for the current to increase from its initial value to some arbitrary value, it is not necessary to find a number of points on the current-vs-time curve.

Therefore, in summary, the step-by-step procedure in solving a nonlinear differential equation by this method is:

(1) Normalize the given equation so that the phase-plane plot lies on the graph paper. This is done by the same method used to find the computer solution.

(2) Eliminate all integrals by differentiation.

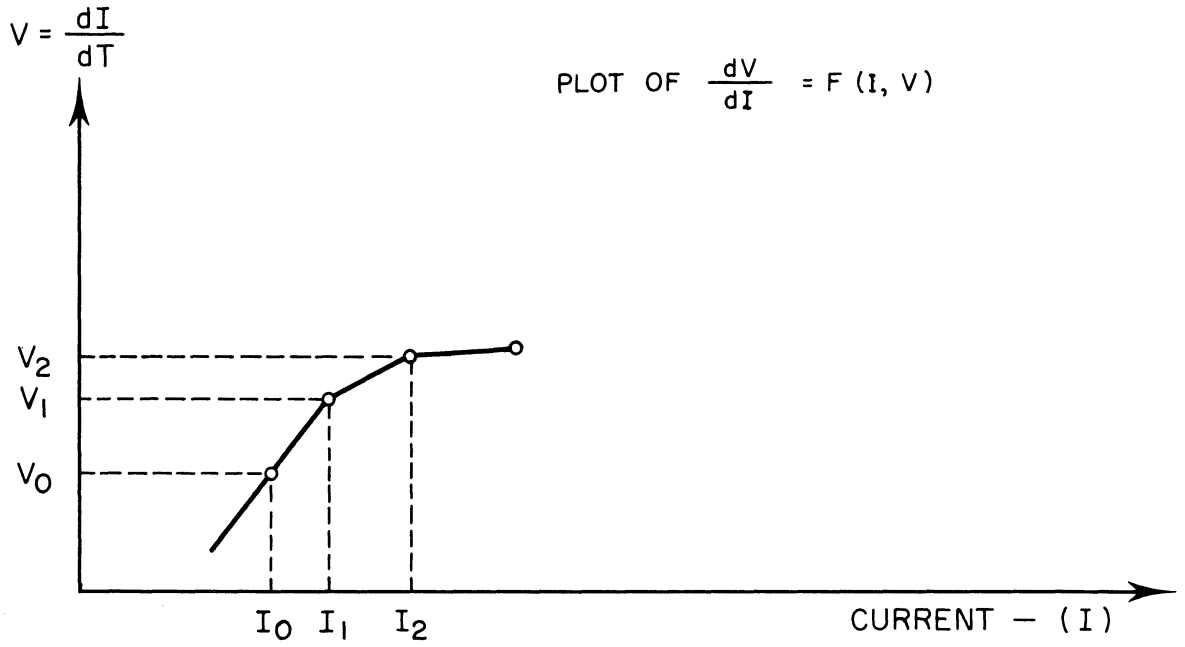

FIG. A-II-1 FIGURE SHOWS METHOD OF CONSTRUCTING PHASE-PLANE PLOT.

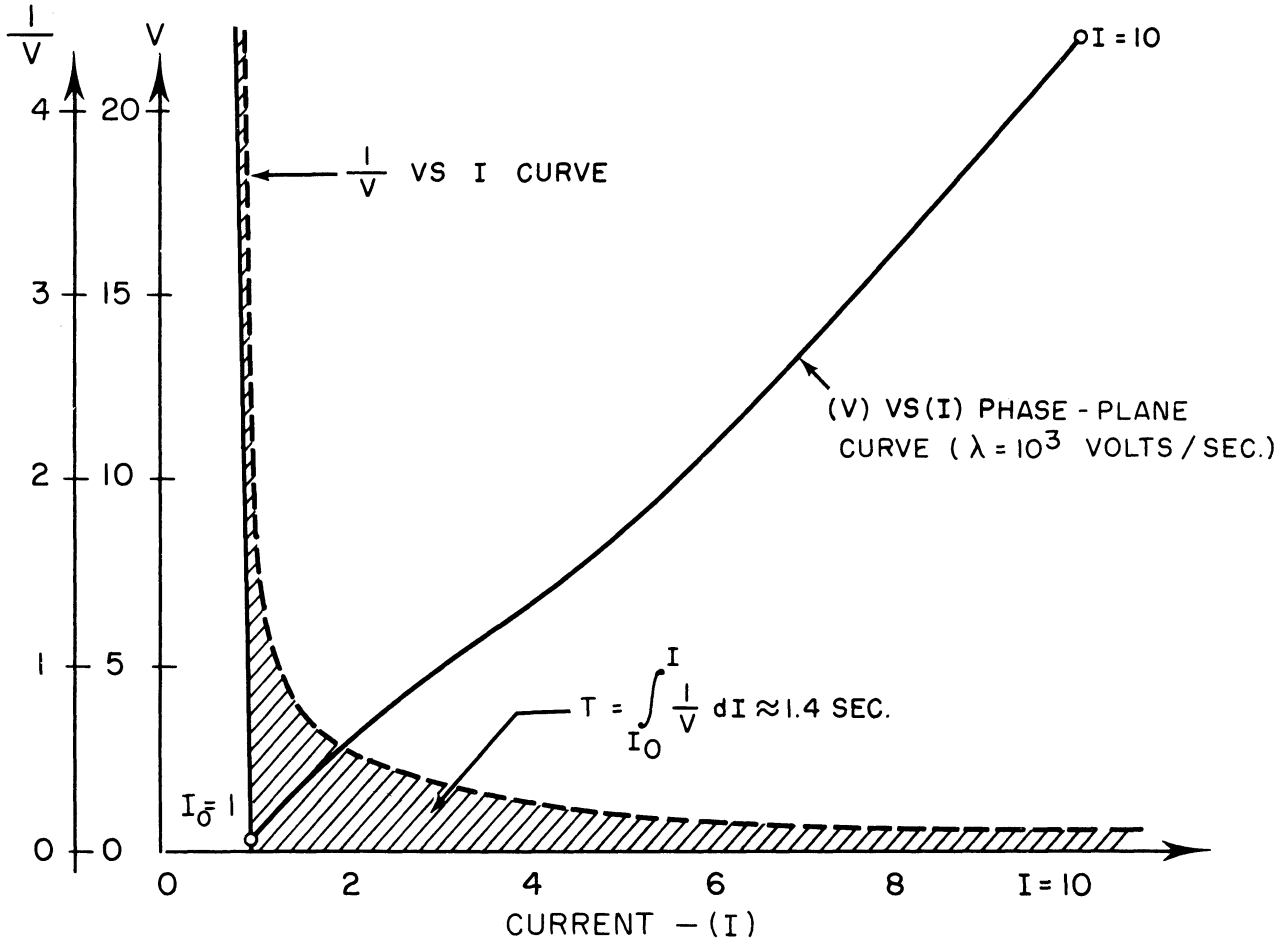

FIG. A-II-2 PHASE - PLANE PLOT OF EQUATION 12.3. ($\lambda = 10^3$)

(3) If the given equation is nth order, then represent it by n first-order differential equations.

(4) Finally, eliminate the independent variable by appropriate substitutions.

(5) From the equation obtained in step 4, construct a phase-plane plot.

(6) After the velocity-vs-distance or (dI/dT = V)-vs-I curve of step 5 is drawn, the (1/V)-vs-I curve is constructed.

(7) The value of the independent variable for each value of dependent variable is then found by calculating the area under the (1/V)-vs-I curve of step 6.

A phase-plane plot of Eq. A-II-3 is shown in Fig. A-II-2 for $\lambda = 10^3$ volts/sec. Also, the time for the current I to increase from the normalized values of $I_o = 1$ to $I = 10$ is found, corresponding to a current change of $i_o = 10^{-9}$ amp to $i = 10^{-8}$ amp of the original equation (A-II-1).

APPENDIX III

ANALOG COMPUTER TECHNOLOGY

Figure 7.2 in Section 7 represented an analog computer setup used to simulate Eq. 7.2. The following is a brief description of the setup.

Functions of various symbols (see Fig. A-III-1):

(1) Integrater: The output voltage is equal to the time integral of the input voltage.

(2) Adder: The output voltage is equal to the sum of the input voltages multiplied by some constant usually greater than 1.

(3) Potentiometer: Used when voltage is to be multiplied by a constant less than 1.

(4) Servo-Multiplier: An electromechanical device which is capable of multiplying two variables.

(5) Photo-Former: Consists of a cathode-ray tube with a short persistence screen, an outline (opaque on one side of the line) of the desired function in front of the screen, and a photo-multiplier tube in front of the screen. The cathode-ray spot in normal operation is positioned along the x axis by a voltage representing the input or forcing function; the output of the photo-multiplier tube is connected through high-gain amplifiers to the vertical deflection plates of the cathode-ray tube, and so drives the spot to the line separating the opaque and clear portions of the outline, i.e., the function shape. The voltage required to hold the spot on this line is a direct measure of the y value of the function at that point.

In simulating Eq. 7.2 by computer, the dependent and independent variables are first normalized into computer units. The computer setup is then connected as shown in Fig. 7.2 with the appropriate initial conditions. The λt voltage is then applied to the setup and the voltage representing the variable (i) is recorded. Figure 7.3 shows a typical representation of the variable from a computer solution.

INTEGRATOR:

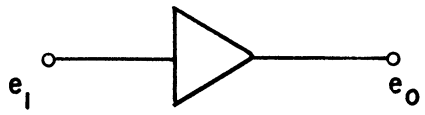

$$e_0 = -\int e_1 \, dt$$

ADDER:

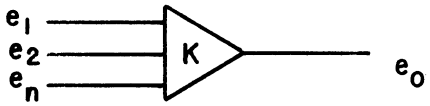

$$e_{OUT} = -K \sum_{i=1}^{n} e_i$$

MULTIPLIER:

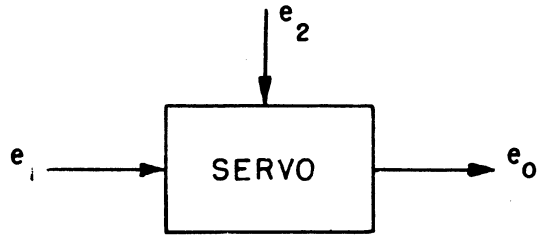

$$e_0 = -\frac{e_1 e_2}{100}$$

PHOTO-FORMER

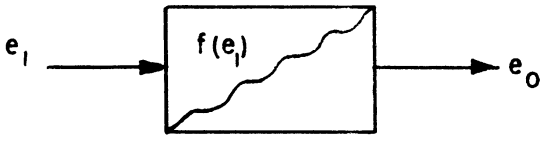

$$e_0 = f(e_1)$$

FIG. A-III-I ANALOG COMPUTER TECHNOLOGY

APPENDIX IV

GRID-TO-CATHODE STATIC CHARACTERISTICS

In Fig. 3.3 of Section 3 a sketch of the static characteristics of the grid-to-cathode gap of a typical QF-391 gas tetrode is shown. These static characteristics were obtained with the setup shown in Fig. A-IV-1.

The values of resistance used in the second grid circuit will affect the static characteristics of the first grid, but for the purposes of this study, was held constant.

To obtain the static characteristic of the first grid of a tube, we proceeded in the following manner (Fig. A-IV-1). E_g was increased until about 1×10^{-9} amp were indicated by the Keithley electrometer (i_o). Then E_2 and E_1 were adjusted until zero current flowed through this shunt circuit. The value of i_o was thus the true grid current, and the $E_2 + E_1$ was the grid-to-cathode voltage. We then proceeded increasing E_g and i_o, keeping i_x equal to zero. In this way the grid-cathode static characteristic was obtained. The maximum error in reading i_o was estimated to be $\pm .01 \times 10^{-9}$ amp. The minimum current which could be detected by i_x was $\pm 10^{-12}$ amp. Therefore, the maximum error in determining e_g was $i_x R = 10^{-12} \times 10^{10} = .01$ volt. This accuracy was reasonable for our purposes.

All runs were made in a shielded box using Keithley battery-powered electrometers and Victoreen Hi-Meg resistors. The fact that consistent, reproducible results were obtained lent confidence that the resulting curves were meaningful. A typical plot is shown (Fig. A-IV-2) where DOFL data (for the same tube) are shown for comparison. The agreement is remarkably good, considering that the curves were taken in different laboratories independently.

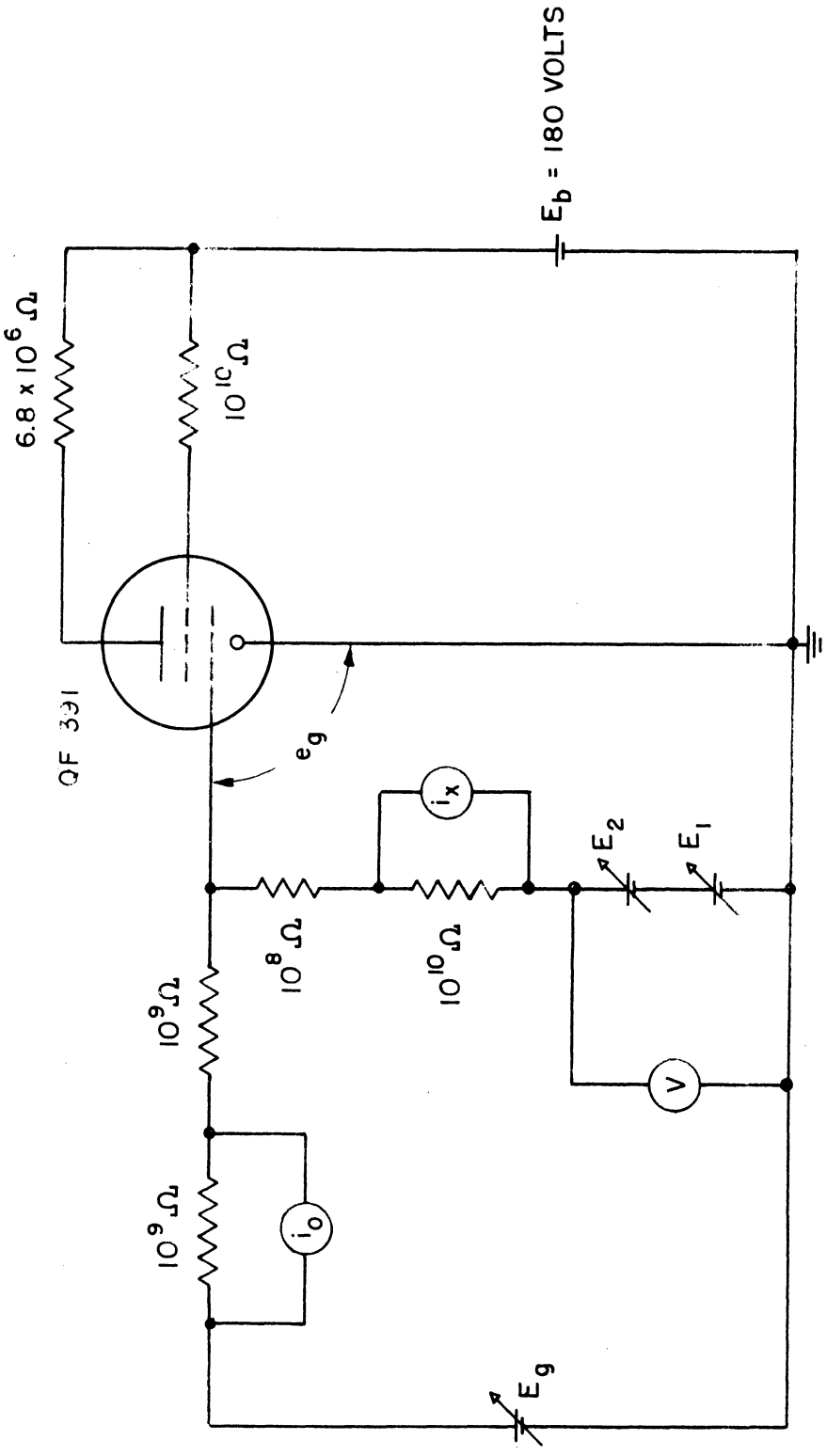

FIG. A-IV-1 GRID-CATHODE STATIC-CHARACTERISTIC SETUP

i_o – INDICATED BY KEITHLEY ELECTROMETER
i_x – INDICATED BY KEITHLEY ELECTROMETER
E_2-0-150 VOLTS E_1-0-4 VOLTS
V – VOLTMETER

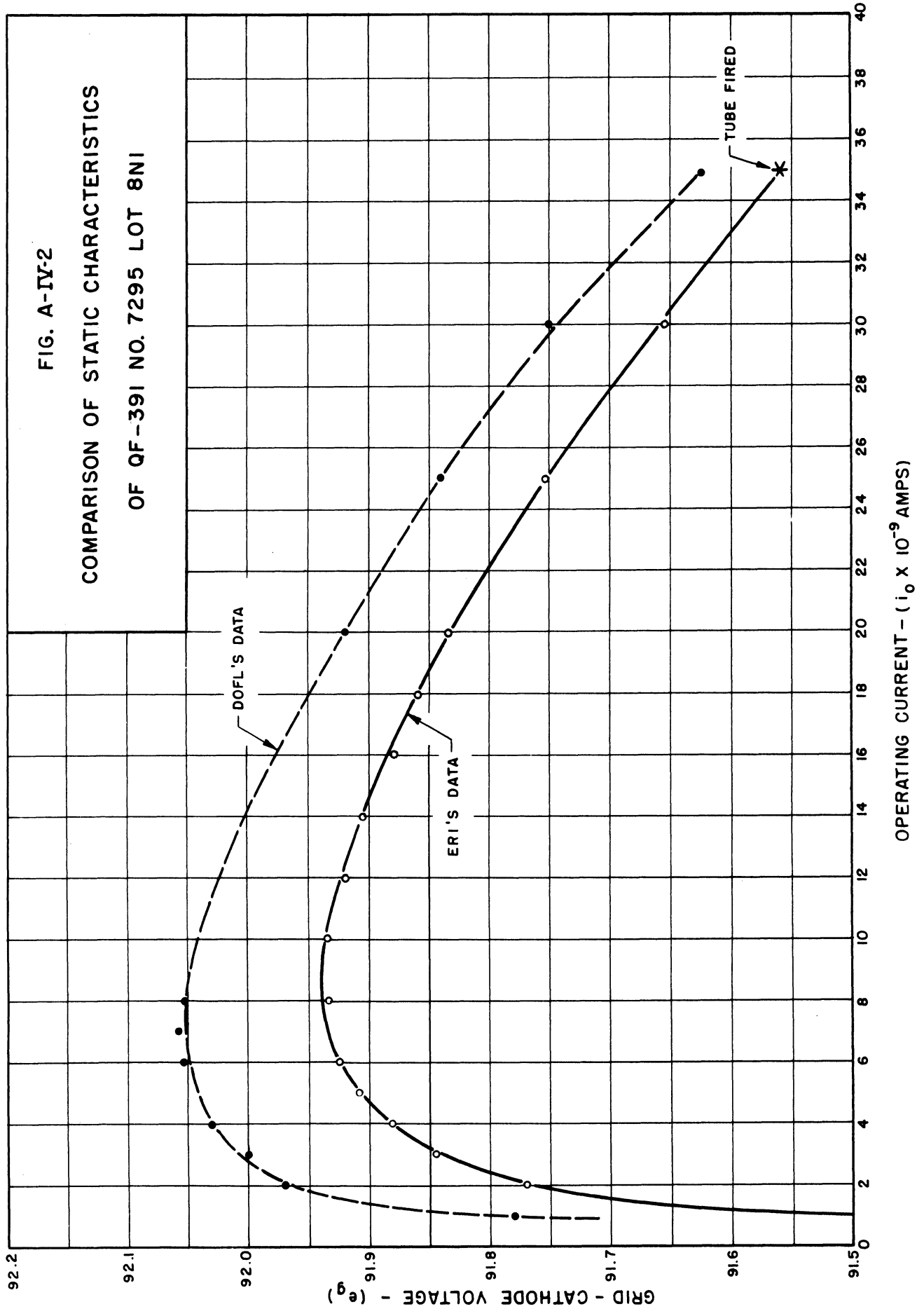
FIG. A-IV-2
COMPARISON OF STATIC CHARACTERISTICS
OF QF-391 NO. 7295 LOT 8NI
DOFL'S DATA
ERI'S DATA
TUBE FIRED
GRID - CATHODE VOLTAGE - (e_g)
92.2
92.1
92.0
91.9
91.8
91.7
91.6
91.5
OPERATING CURRENT - (i_o X 10^{-9} AMPS)
0
2
4
6
8
10
12
14
16
18
20
22
24
26
28
30
32
34
36
38
40